# Postnatal activation of TLR4 in astrocytes promotes excitatory synaptogenesis in hippocampal neurons

Yi Shen,[1,2*] Huaping Qin,[1,2*] Juan Chen,[1,2] Lingyan Mou,[1,2] Yang He,[1,2] Yixiu Yan,[4] Hang Zhou,[1,2] Ya Lv,[4] Zhong Chen,[3] Junlu Wang,[4] and Yu-Dong Zhou[1,2]

[1]Department of Neurobiology, Institute of Neuroscience and [2]Collaborative Innovation Center for Brain Science, Key Laboratory of Medical Neurobiology of the Ministry of Health of China, Zhejiang University School of Medicine, Hangzhou, 310058, China
[3]Department of Pharmacology, Institute of Neuroscience, Key Laboratory of Medical Neurobiology of the Ministry of Health of China, Zhejiang University School of Medicine, Hangzhou 310058, China
[4]Department of Anesthesiology, The First Affiliated Hospital of Wenzhou Medical University, Wenzhou 325000, China

Astrocytes are critical in synapse development, and their dysfunction in crucial developmental stages leads to serious neurodevelopmental diseases, including seizures and epilepsy. Immune challenges not only affect brain development, but also promote seizure generation and epileptogenesis, implying immune activation is one of the key factors linking seizures and epilepsy to abnormal brain development. In this study, we report that activating astrocytes by systemic lipopolysaccharide (LPS) challenges in the second postnatal week promotes excitatory synapse development, leading to enhanced seizure susceptibility in mice. Toll-like receptor 4 (TLR4) activation in astrocytes increased astrocytic extracellular signal–related kinase 1/2 (Erk1/2) and phospho-Erk1/2 levels in a myeloid differentiation primary response protein 88 (MyD88)–dependent manner. Constitutively activating Erk1/2 in astrocytes was sufficient to enhance excitatory synaptogenesis without activating TLR4. Deleting MyD88 or suppressing Erk1/2 in astrocytes rescued LPS-induced developmental abnormalities of excitatory synapses and restored the enhanced seizure sensitivity. Thus, we provide direct evidence for a developmental role of astrocytes in shaping a predisposition to seizure generation.

## Introduction

Astrocytes, a major class of glial cells in the central nervous system (CNS), actively regulate axon guidance, synapse formation and maturation, synapse function and plasticity, and neuronal survival during development (Eroglu and Barres, 2010; Clarke and Barres, 2013; Fields et al., 2015; Haydon and Nedergaard, 2015). Disrupting astrocyte activities and functions in crucial developmental stages leads to serious neurodevelopmental dysfunctions, including seizures and epilepsy, which are often a comorbidity of many neurodevelopmental diseases (e.g., Rett syndrome, autism, and Fragile X syndrome; Molofsky et al., 2012; Sloan and Barres, 2014; Chung et al., 2015). The highest incidence of seizures occurs in early life (Rakhade and Jensen, 2009), further implicating a developmental origin of seizure activities. Thus, elucidating how astrocytes developmentally regulate neuronal and circuit excitability is of particular importance to understanding and treating childhood seizures and epilepsy.

Increasing evidence supports brain inflammation contributes to the etiopathogenesis of seizures (Maroso et al., 2010; Vezzani et al., 2015). As one of the key resident cell types in the CNS mediating inflammatory responses (Lampron et al., 2013), mature astrocytes are known to be associated with seizure generation and epileptogenesis (Wetherington et al., 2008; Devinsky et al., 2013; Robel and Sontheimer, 2016). Upon immune activation, astrocytes become activated with changes in their morphology, proliferation, and molecular expression (Burda and Sofroniew, 2014). This reactive astrogliosis is a hallmark of multiple brain diseases, including epilepsy (Devinsky et al., 2013). In the epileptic foci, reactive astrocytes fail to buffer extracellular $K^+$ and exhibit a reduced glutamate uptake (Djukic et al., 2007; Coulter and Steinhäuser, 2015), resulting in a profound increase in neuronal excitability. Reactive astrogliosis induced by conditional deletion of β1-integrin in astrocytes is sufficient to impair astrocytic glutamate uptake, causing spontaneous seizure activities (Robel et al., 2015). Diminished

*Y. Shen and H. Qin contributed equally to this paper.

Correspondence to Yu-Dong Zhou: yudongzhou@zju.edu.cn; or Junlu Wang: wangjunlu973@163.com

Abbreviations used: ACM, astrocyte-conditioned medium; ACSF, artificial cerebrospinal fluid; A/LPS, astrocyte-conditioned medium from lipopolysaccharide-treated astrocyte; ANOVA, analysis of variance; CNS, central nervous system; DIV, days in vitro; E, embryonic day; ERK, extracellular signal–related kinase; IUE, in utero electroporating; LPS, lipopolysaccharide; LPS-RS, lipopolysaccharide from *Rhodobacter sphaeroides*; MEK, MAPK kinase; mEPSC, miniature excitatory postsynaptic current; mIPSC, miniature inhibitory postsynaptic current; NDS, normal donkey serum; NF-κB, nuclear factor-κB; p, phosphorylated; P, postnatal day; PTZ, pentylenetetrazol; TLR4, Toll-like receptor 4; TSP, thrombosponding; TTX, tetrodotoxin; WT, wild-type.



The Rockefeller University Press $30.00
J. Cell Biol. Vol. 215 No. 5 719–734
https://doi.org/10.1083/jcb.201605046

glutamate uptake and reduced expression of glutamine synthetase in reactive astrocytes impair glutamine synthesis, leading to a decrease in neuronal γ-aminobutyric acid production and a subsequent increase in network excitability (Ortinski et al., 2010). Although we are starting to understand how reactive astrocytes regulate neuronal and network excitability, we know little about how maturing astrocytes alter neuronal excitability through noncell autonomous mechanisms and/or tilt the balance of excitation and inhibition via shaping the central circuit upon immune activation in the developing brain.

Unlike mature astrocytes, maturing astrocytes in the developing brain have limited $K^+$ buffering capacity (Seifert et al., 2009) and slow glutamate uptake capability (Diamond, 2005). Disturbing astrocyte activities during postnatal development may have minimal effect on the neuronal microenvironment and hence no direct consequence on neuronal excitability. In contrast, maturing astrocytes are actively involved in synaptogenesis (Christopherson et al., 2005; Eroglu et al., 2009; Allen et al., 2012) and synapse elimination (Chung et al., 2013) during postnatal development. Predisposing risk factors such as immune activation impairing astrocyte functions may strongly affect the development of a specific type of synapse, leading to abnormal network excitability. Thus, it will be interesting to study how astrocytes responding to immune activation modulate synapse development, causing a predisposition to seizure generation.

There is a considerable amount of Toll-like receptor 4 (TLR4) expressed in differentiated astrocytes (Zhang et al., 2016). TLR4 plays an essential role in the induction of innate immune responses and has been implicated in epileptogenesis (Maroso et al., 2010). Peripheral TLR4 activation has been shown to disrupt gap junctions among astrocytes, causing mesial temporal lobe epilepsy with sclerosis (Bedner et al., 2015). In this study, we investigated the effects of astrocytic TLR4 activation on synaptogenesis in hippocampal CA1 neurons and seizure susceptibility in young mice during a postnatal period, as well as the underlying signaling pathway initiated by TLR4 activation in astrocytes, to elucidate the critical molecular and cellular mechanisms of astrocytic TLR4 activation in early-life epileptic seizures.

## Results

### Lipopolysaccharide (LPS)-induced enhancement of seizure susceptibility in juvenile mice is concurrent with an increase in excitatory synaptic transmission

To determine whether there is a critical postnatal period during which systemic LPS challenges affect seizure susceptibility, we examined pentylenetetrazol (PTZ)–induced seizures in postnatal day (P) 21 mice treated with LPS for 3 consecutive days from P10–12 or in adult mice treated with LPS from P70–72. In comparison to the prior saline treatments, the prior LPS treatments significantly reduced the onset and prolonged the duration of PTZ-induced convulsions in P21 mice (Fig. 1 A). The prior LPS challenges, however, did not affect the onset and the duration of PTZ-induced seizures in adult mice (P70–72; Fig. 1 B). Moreover, PTZ-induced convulsions remained increased in adult mice previously treated with LPS from P10–12 (Fig. 1 C), indicating that such an increase is a long-lasting phenomenon. As brain TLR4 can be directly activated by circulating LPS or indirectly by LPS-induced peripheral inflammatory mediators, we next tested the effect of peripheral LPS injections on PTZ-induced seizures in young TLR4 knockout (*TLR4*$^{-/-}$) mice. We observed that LPS had no effect on seizure susceptibility in young *TLR4*$^{-/-}$ mice (Fig. S1, A and B), suggesting that TLR4 activation renders young animals more prone to PTZ-induced seizures.

Hippocampal circuitry is involved in initiating and spreading epileptic seizures. We then investigated whether LPS treatments in the second postnatal week could alter synaptic function and development in the hippocampus. In comparison to saline treatments, LPS treatments from P10–12 significantly increased the frequency (Fig. 1, D and F) and the amplitude (Fig. 1, D and G) of miniature excitatory postsynaptic currents (mEPSCs) recorded from CA1 pyramidal neurons in P14 mice. LPS failed to significantly change mEPSC frequency (Fig. 1, E and H) and amplitude (Fig. 1, E and I) when injected in adult mice. Both early and late LPS challenges had no effect on the kinetics of mEPSCs recorded from CA1 pyramidal neurons (unpublished data). Furthermore, LPS treatments from P10–12 notably promoted dendritic branching (Fig. 1, J–L) and increased spine density (Fig. 1 M) in CA1 pyramidal neurons from P14 mice. However, LPS did not affect dendritic branching and spine density in CA1 pyramidal neurons in adult mice (Fig. 1, J–M). Together, these results indicate that systemic LPS treatments in the second postnatal week promote excitatory synapse development with a concurrent enhancement of seizure sensitivity.

### LPS-induced promotion of excitatory synapse development requires astrocytes

Both astrocytes and microglia are considered as the major targets for immune responses in the CNS. Therefore, we next investigated if LPS treatments were able to alter activation of astrocytes and microglia in the hippocampal CA1 areas of P14 and adult mice. Hippocampal activation of glial cells was estimated by calculating the relative mean fluorescence intensities of the glia markers and the normalized numbers of fluorescent cells per unit area. We found that there was an increase in GFAP-positive cell number and fluorescence intensity in LPS-treated P14 mice in comparison with saline-treated controls (Fig. 2, A and B). LPS, however, failed to significantly alter Iba-1–positive cell number and fluorescence intensity in LPS-treated P14 mice in comparison with saline-treated ones (Fig. 2, C and D). By contrast, LPS challenges to adult mice resulted in an increase in the number and fluorescence intensity of Iba-1–positive cells (Fig. 2, G and H), whereas the number and fluorescence intensity of GFAP-positive cells did not change (Fig. 2, E and F). In addition, LPS-induced increase in astrocyte activation was not observed in young *TLR4*$^{-/-}$ mice (Fig. S1 C). Furthermore, systemic LPS challenges significantly enhanced TLR4 expression in astrocytes in juvenile mice (Fig. 2 I; Hickey et al., 2011) but not in adult mice (Fig. 2 J), although the basal expression of TLR4 in astrocytes was limited in the hippocampus (the percentage of TLR4-positive astrocytes: 11.8 ± 0.6% for the juvenile group, $n$ = 10; 9.6 ± 0.5% for the adult group, $n$ = 10). The results indicated that peripheral LPS selectively increased astrocyte activation in the hippocampus of mice in the second postnatal week and implicated astrocytic TLR4 activation might be involved in the LPS-induced astrogliosis in the hippocampus in mice during this critical period.

It has been shown that TLR4 activation promotes epileptogenesis via regulating neuronal survival, development, and

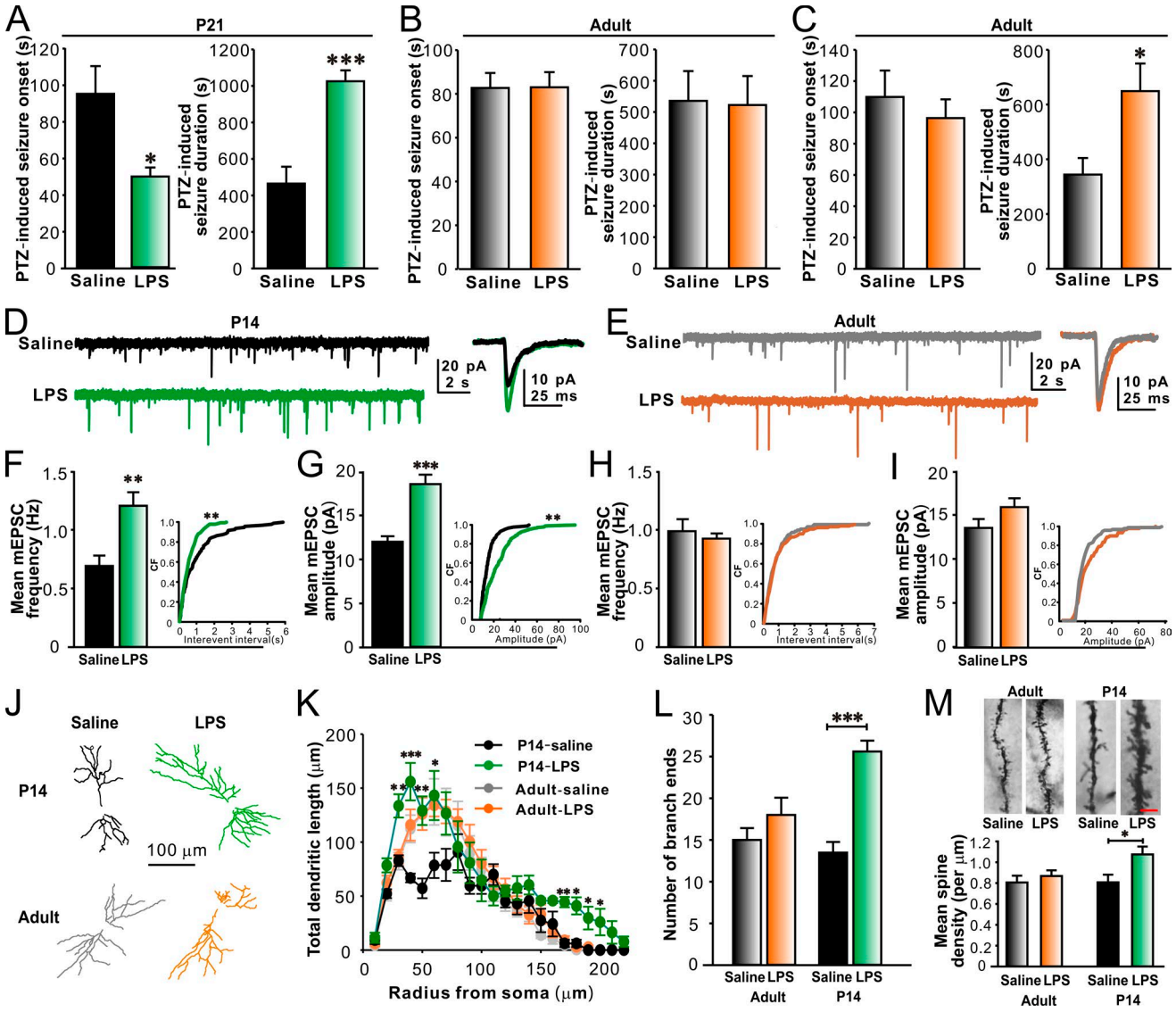


Figure 1. **LPS increases PTZ-induced seizure susceptibility and promotes synapse development in CA1 pyramidal neurons in juvenile mice.** Prior LPS injections significantly reduced the onset and prolonged the duration of PTZ-induced convulsions in P14 mice (A) but not in adult mice (B). *n* = 8, 8, 9, and 9 for P21 saline, P21 LPS, adult saline, and adult LPS groups, respectively. (C) LPS injections in early-life (P10–12) did not affect the onset but significantly prolonged the duration of PTZ-induced convulsions in adult mice (P70–72). *n* = 8 for each group. Representative traces of mEPSC recordings from P14 mice (D) and adult mice (E). LPS increased mEPSC frequency and amplitude in CA1 pyramidal neurons in P14 mice (F and G) but not in adult mice (H and I). *n* = 10, 10, 9, and 9 for P14 saline, P14 LPS, adult saline, and adult LPS groups, respectively. (J) Representative reconstructions of CA1 pyramidal neurons from P14 (top) and adult (bottom) mice treated with saline or LPS. (K) Sholl analysis of CA1 pyramidal neuron dendritic arbor. *n* = 10 for each group. (L) Quantification of the number of dendritic branch ends. *n* = 10 for each group. (M) Representative images (top) and quantification of mean spine density (bottom) showing an increased spine density in CA1 pyramidal neurons in P14 mice treated with LPS. Bar, 8 μm. *n* = 8, 9, 9, and 10 for P14 saline, P14 LPS, adult saline, and adult LPS groups, respectively. *, $P < 0.05$; **, $P < 0.01$; ***, $P < 0.001$ (cumulative distributions in F and G, Kolmogorov-Smirnov test; in K, two-way ANOVA with the post hoc Holm-Sidak test; in other panels, *t* test). Data are mean ± SEM. CF, cumulative frequency.

function (Rodgers et al., 2009; Maroso et al., 2010). Therefore, to further determine if early TLR4 activation in astrocytes regulates synapse development in the hippocampus, we established primary culture methods for mouse hippocampal neurons and astrocytes, as well as an astrocyte-neuron co-culture paradigm. The mouse astrocyte cultures contained very few microglia, as estimated by immunostaining with GFAP and Iba-1 and Western blotting for GFAP and Iba-1 (as described in the Materials and methods). We then compared the proportion of dead cells found in control cultures with those in cultures exposed to 1 μg/ml LPS for 48 h using propidium iodide staining. No significant change could be found in the numbers of survival cells in control and LPS-exposed cultures (control group: 23,238 ± 2,390 cells/cm$^2$; LPS group: 21,767 ± 1,753 cells/cm$^2$; *n* = 10 coverslips from three cultures for both groups), indicating LPS exposure did not affect cell viability.

We then examined the effects of LPS on synaptogenesis and dendritic branching of neurons from primary cultures or astrocyte-neuron co-cultures (LPS exposures at 8 to 9 d in vitro [DIV8 to 9], DIV10 to 11, or DIV13 to 14; Fig. 3 A). We found LPS treatment caused dramatic increases in the densities of PSD95 puncta (Fig. 3, B and C) and synaptophysin/PSD95 colocalized puncta (Fig. 3, B and D) in neurons co-cultured with astrocytes at DIV12 and 15 after a prior exposure of LPS

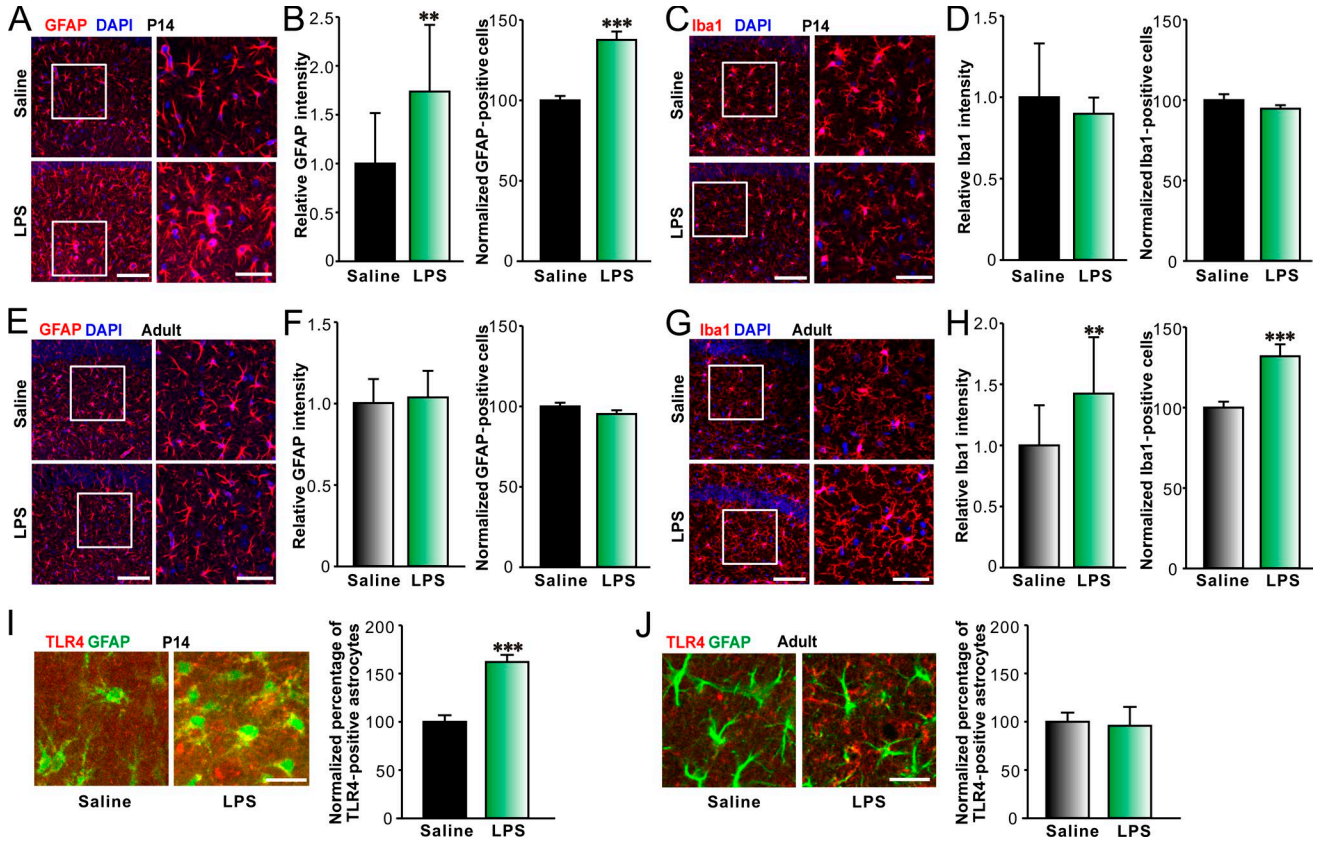


Figure 2. **LPS selectively increases astrocyte activation in hippocampal CA1 area in young mice.** Representative images of immunohistostaining of GFAP (red) and DAPI (blue; A) or Iba-1 (red) and DAPI (blue; C) and quantification of relative intensity of GFAP (B, left) or Iba-1 (D, left) and normalized GFAP- (B, right) or Iba-1–positive (D, right) cell numbers per unit area in hippocampal CA1 area of P14 mice treated with saline or LPS showing astrocyte activation upon LPS treatment in P14 mice. Bars: (left) 100 µm; (right) 50 µm. *n* = 13 for each group. Representative images of immunohistostaining of GFAP (red) and DAPI (blue; E) or Iba-1 (red) and DAPI (blue; G) and quantification of relative intensity of GFAP (F, left) or Iba-1 (H, left) and normalized GFAP- (F, right) or Iba-1–positive (H, right) cell numbers in hippocampal CA1 area of adult mice treated with saline or LPS showing microglia activation upon LPS treatment in adult mice. Bars: (left) 100 µm; (right) 50 µm. *n* = 12 for each group. Representative images (left) of immunohistostaining of colocalization of TLR4 (red) and GFAP (green) in hippocampal CA1 area of P14 (I) and adult (J) GFAP-GFP mice treated with saline or LPS and quantification of the percentage of TLR4-positive astrocytes (right). Bars, 25 µm. *n* = 10 for each group. **, P < 0.01; ***, P < 0.001 (*t* test). Data are mean ± SEM.

for 48 h. However, LPS did not alter the densities of PSD95 puncta (Fig. 3, B and C) and synaptophysin/PSD95 colocalized puncta (Fig. 3, B and D) in neurons alone at DIV10, 12, and 15. LPS also significantly increased the dendritic length (Fig. 4, A and B) and branch number (Fig. 4, A and C) in neurons co-cultured with astrocytes at DIV12 and -15. LPS-induced changes in dendritic pattern of neurons in co-cultures were mainly manifested with more ramified second and third dendritic branches (Fig. 4, D–I). The effects of LPS on synapse formation and dendritic branching in neurons from co-cultures were blocked by TLR4 antagonist LPS from *Rhodobacter sphaeroides* (LPS-RS; unpublished data). In addition, LPS also increased the frequency and amplitude of mEPSCs recorded from neurons in co-cultures at DIV15 (Fig. S2, A–C), but did not affect miniature inhibitory postsynaptic currents (mIPSCs; Fig. S2, D–F), indicating LPS selectively promoted excitatory synaptic function. Taken together, these results illustrated that astrocytes contributed to LPS-induced excitatory synaptogenesis and dendritic branching in hippocampal neurons and suggested this LPS-induced facilitation of excitatory transmission in the second postnatal week might enhance PTZ-induced seizure susceptibility in mice.

### LPS-induced promotion of excitatory synapse development is specifically mediated by TLR4–MyD88 signaling pathway in astrocytes

TLR4 is widely expressed in various cell types in the brain, including astrocytes and neurons. To determine the specific signaling pathway in astrocytes that promoted synaptic and neuronal development, we first examined LPS-induced TLR4 activation in astrocyte and neuron cultures. Western blots showed that LPS exposure notably increased TLR4 expression in astrocytes, neurons in co-cultures, and neurons alone (Fig. 5 A), and the increased TLR4 expressions were blocked by TLR4 antagonist LPS-RS (Fig. 5 A). One of the key downstream adaptors of TLR4 activation is MyD88 (myeloid differentiation primary response protein 88), and TLR4 activation may result in MyD88-dependent or -independent signaling pathways in different cell types (Okun et al., 2011). Thus, we next tested MyD88 expression in response to LPS treatment in astrocytes and neurons. LPS exposure specifically increased MyD88 expression in astrocytes, but not in neurons from co-cultures or primary cultures (Fig. 5 B). These results implicate that astrocytes and neurons may undergo distinct

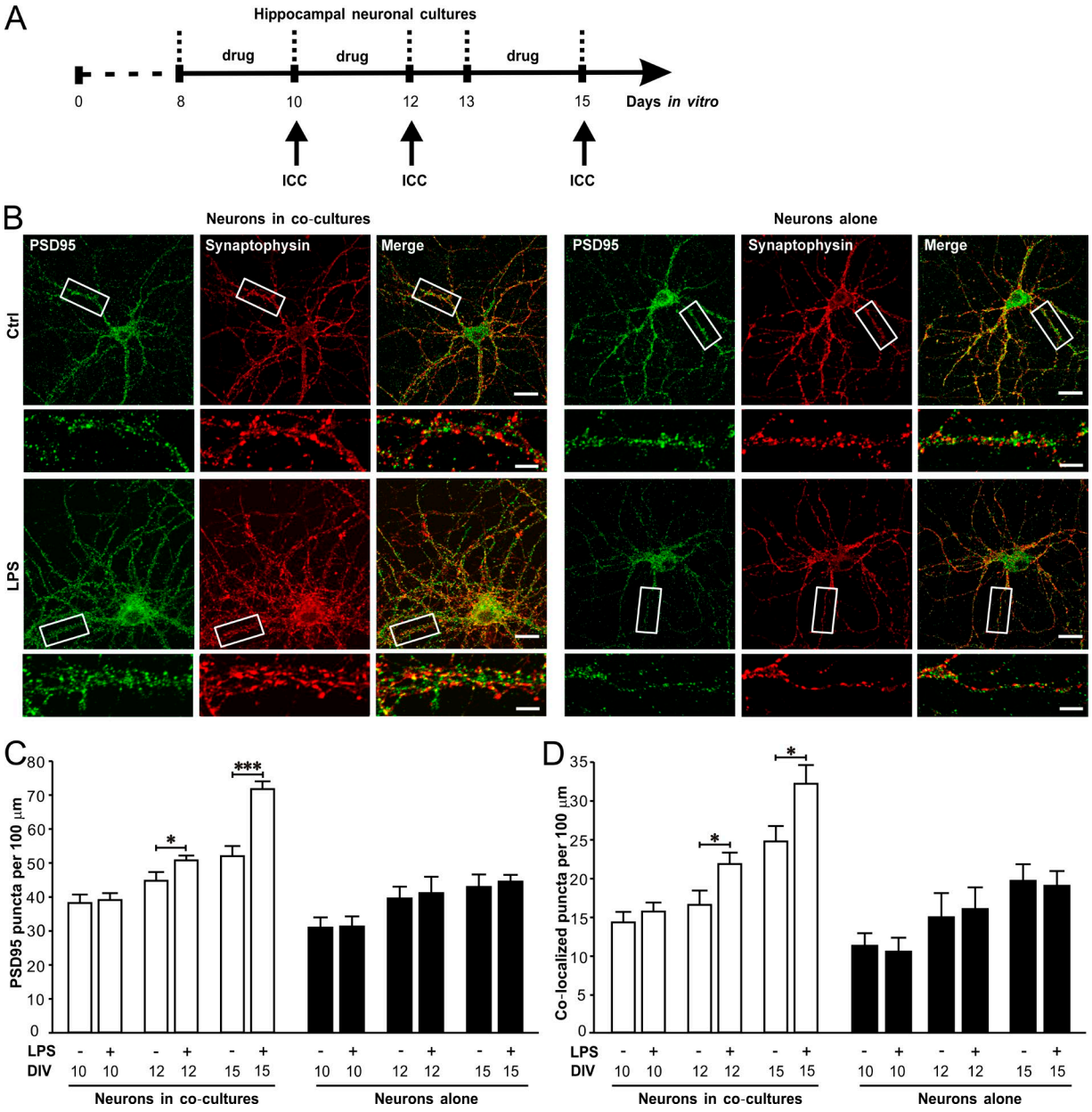


Figure 3. **LPS promotes synaptogenesis in hippocampal neurons in astrocyte-neuron co-cultures.** LPS (1 µg/ml) was added in astrocyte-neuron co-cultures or neuron cultures for 48 h before immunocytochemistry. (A) Schematics of experimental procedures. (B) Representative images of immunostaining of PSD95 (green) and synaptophysin (red) in neurons co-cultured with astrocytes (left) and neurons alone (right). Bars: 20 µm; (magnification) 5 µm. Quantification of PSD95 puncta (C) and PSD95/synaptophysin colocalized puncta (D) in neurons co-cultured with astrocytes at DIV12 and DIV15. $n = 30$ for each group. Ctrl, control; ICC, immunocytochemistry. *, $P < 0.05$; ***, $P < 0.001$ (*t* test). Data are mean ± SEM.

signaling events after TLR4 activation. Astrocytic TLR4 activation may recruit the key adaptor protein MyD88, whereas MyD88 is not involved in neuronal TLR4 activation. Because we used a noncontact co-culture system for neurons and astrocytes (see details in the Materials and methods), we further exposed neuron cultures with astrocyte-conditioned medium (ACM) from LPS-treated astrocyte (A/LPS) to test whether A/LPS affects synaptic and neuronal development. A/LPS elevated synapse formation and dendritic branching in primarily cultured neurons alone (Fig. S3).

To further confirm that MyD88 is recruited after TLR4 activation in astrocytes and regulates synapse development, we established co-cultures of astrocytes from *TLR4*$^{-/-}$ or myeloid differentiation primary response protein 88 knockout (*MyD88*$^{-/-}$) mice and neurons from wild-type (WT) mice. LPS exposure did not elevate MyD88 expression in *TLR4*$^{-/-}$ astrocytes and WT neurons co-cultured with *TLR4*$^{-/-}$ astrocytes (Fig. 5 C). LPS also failed to promote synaptogenesis in WT neurons co-cultured with *TLR4*$^{-/-}$ (Fig. 5, D and E) or *MyD88*$^{-/-}$ astrocytes (Fig. 5, F and G). In contrast, LPS significantly promoted synaptogenesis and dendritic branching in WT, *TLR4*$^{+/-}$, and *TLR4*$^{-/-}$ neurons (DIV15) co-cultured with WT astrocytes (Table S1). Together, these data indicate that activation of astrocytic TLR4–MyD88 signaling pathway is necessary for LPS-induced abnormal synapse formation and dendritic pattern in cultured hippocampal neurons.

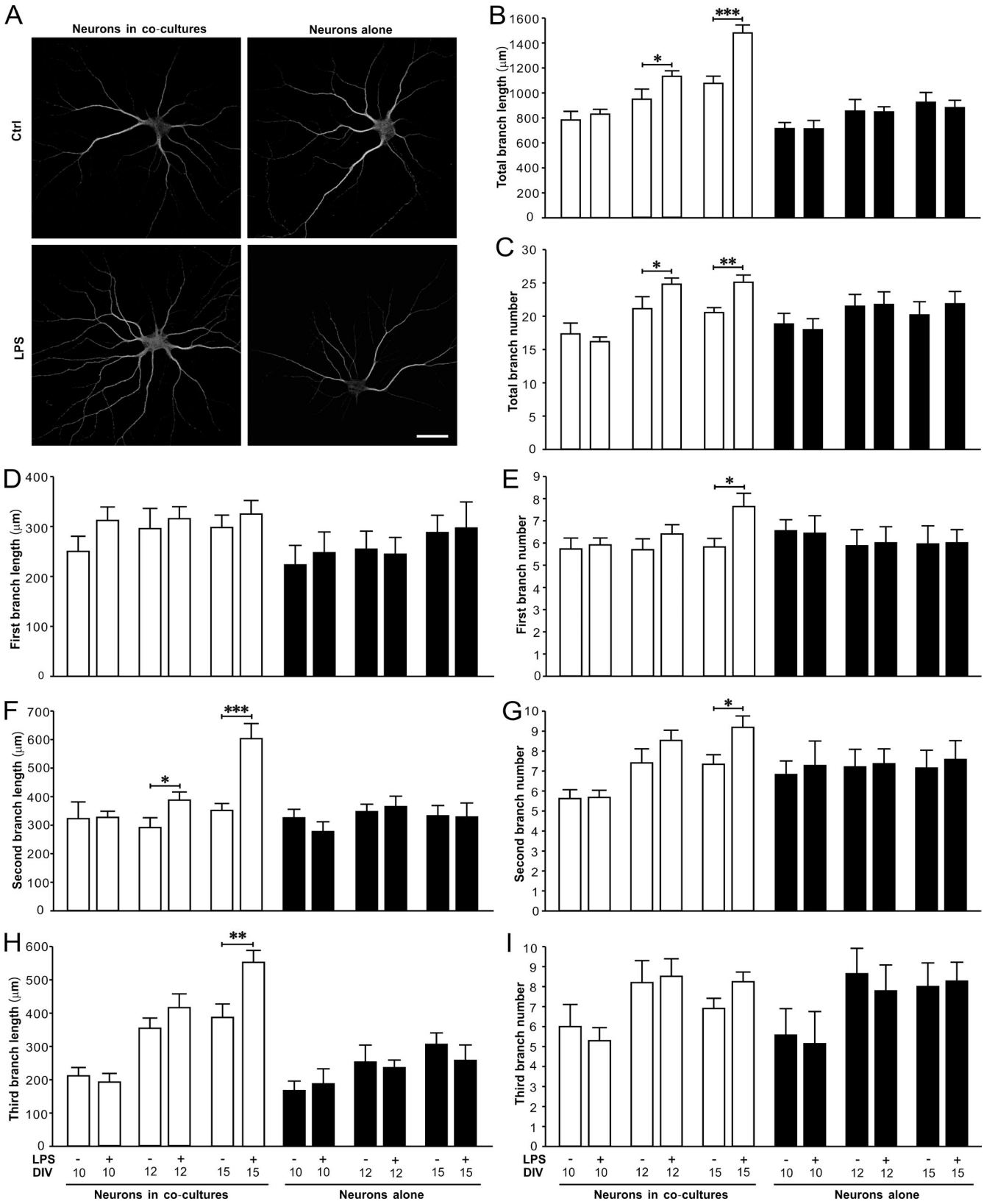


Figure 4. **LPS significantly increases the dendritic branching in hippocampal neurons co-cultured with astrocytes.** (A) Representative images of immunostaining of MAP2 in neurons co-cultured with astrocytes (left) and neurons alone (right). Bar, 40 µm. Quantification of the length (B) and number (C) of total dendritic branches. Quantification of the length of the first (D), second (F), and third (H) dendritic branches. Quantification of the number of the first (E), second (G), and third (I) dendrite branches. $n = 30$ for each group. *, $P < 0.05$; **, $P < 0.01$; ***, $P < 0.001$ (*t* test). Data are mean ± SEM.

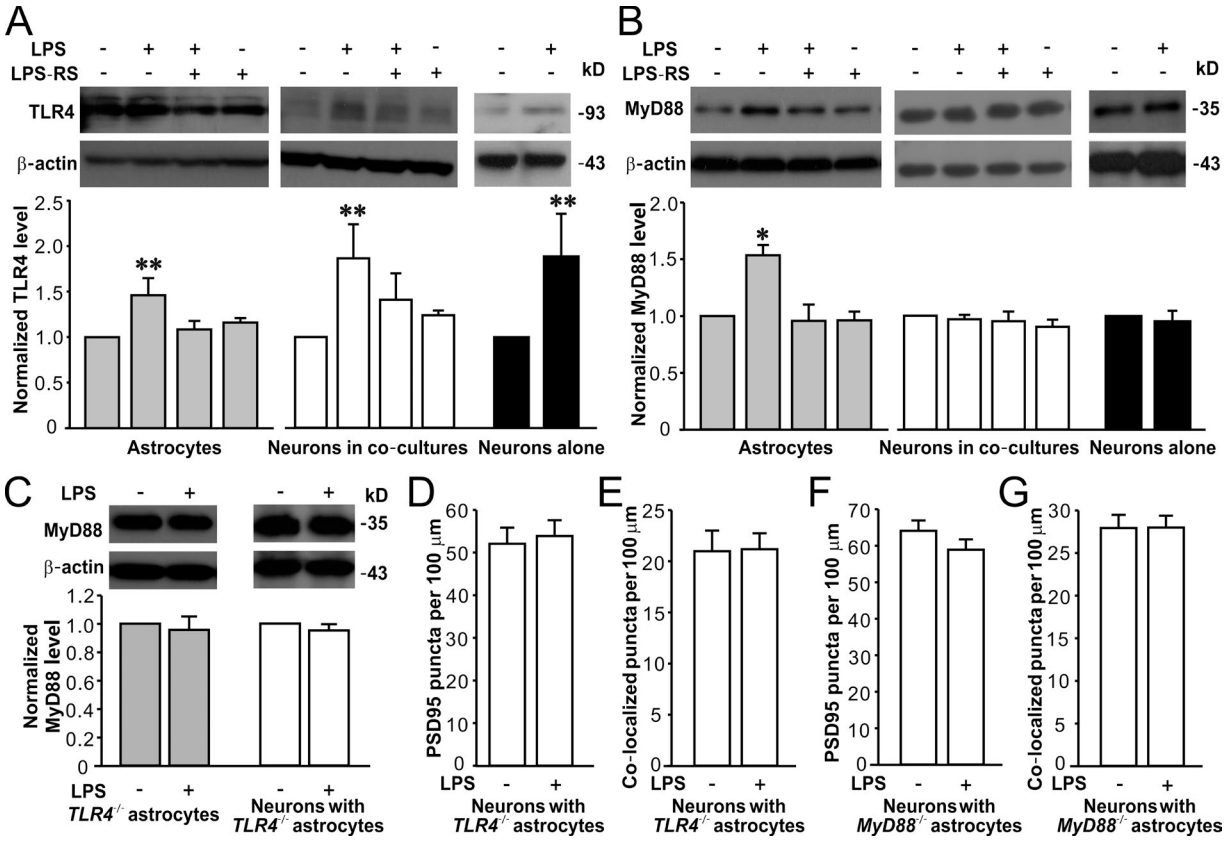


Figure 5. **LPS specifically activates TLR4–MyD88 signaling in astrocytes.** Representative Western blots of TLR4 (A) and MyD88 (B) in astrocytes, neurons in co-cultures (DIV15), and neurons alone (DIV15; top) and quantification of TLR4 (A) and MyD88 (B) expression (bottom). *n* = 4, 4, and 3 for astrocytes, neurons in co-cultures, and neurons alone groups, respectively. (C) Representative Western blots of MyD88 in *TLR4*$^{-/-}$ astrocytes and neurons co-cultured with *TLR4*$^{-/-}$ astrocytes (top) and quantification of MyD88 expression (bottom). *n* = 3 for each group. Quantification of PSD95 puncta (D) and PSD95/synaptophysin colocalized puncta (E) in neurons co-cultured with *TLR4*$^{-/-}$ astrocytes. *n* = 32 in each group. Quantification of PSD95 puncta (F) and PSD95/synaptophysin colocalized puncta (G) in neurons co-cultured with *MyD88*$^{-/-}$ astrocytes. *n* = 29 for each group. β-Actin is shown as a loading control. *, $P < 0.05$; **, $P < 0.01$ (*t* test or one-way ANOVA with the post hoc Dunnett's test). Data are mean ± SEM.

To test if TLR4–MyD88 signaling pathway in astrocytes is involved in LPS-induced enhancement of seizure susceptibility in young mice, we deleted MyD88 in astrocytes by in utero electroporating (IUE) a set of *piggyBac* plasmids targeting astrocytes into *MyD88*$^{flox/flox}$ mice (see details in the Materials and methods; Fig. 6 A). The mean IUE transfection rate was 50.1 ± 8.8% (*n* = 25, ranging from the lowest rate of 35.9% to the highest rate of 71.8%; Fig. 6 A; see details in the Materials and methods). GFP-positive cells in the hippocampus of IUE mice were also positive for s100β (Fig. 6 B), confirming the transfected cells are astrocytes. Approximately 96.1 ± 1.1% of GFP-positive astrocytes were devoid of MyD88 in mice (*n* = 9) electroporated with the *piggyBac* plasmids, whereas MyD88 expression in GFP-positive astrocytes was not affected in mice electroporated with the negative control plasmids (Fig. 6 B). In addition, MyD88 expression was not decreased in microglia in mice electroporated with the *piggyBac* or control plasmids (unpublished data), indicating that MyD88 was specifically ablated in *piggyBac* plasmids-transfected astrocytes. As expected, astrocytic MyD88 deletion inhibited the LPS effects on PTZ-induced seizure susceptibility (Fig. 6, C and D). LPS still increased PTZ-induced convulsions in mice electroporated with the control plasmids (Fig. 6, C and D). In addition, LPS failed to strongly elevate the frequency (Fig. 6, E and F) and amplitude (Fig. 6, E and G) of mEPSCs recorded from CA1 pyramidal neurons in mice with astrocytic MyD88 partially deleted. LPS still significantly increased the frequency (Fig. 6, E and F) and amplitude (Fig. 6, E and G) of mEPSCs recorded from CA1 pyramidal neurons in the control group. These results demonstrate that LPS-induced effects on seizure susceptibility and excitatory synaptic transmission in young animals are dependent on astrocytic MyD88.

### LPS-induced promotion of excitatory synapse development is mediated by a TLR4 signaling pathway that involves extracellular signal–related kinase 1/2 (Erk1/2) activation in astrocytes

Previous studies have reported that stimulation of TLR4 in astrocytes activates the MyD88-dependent pathway, leading to nuclear factor-κB (NF-κB)–induced transcriptional regulation of TNF and MAPK–mediated tyrosine phosphorylation of signal transducer and activator of transcription 1, though MyD88-independent signaling was also found in astrocytes (Gorina et al., 2011; Okun et al., 2011). Therefore, we investigated if MAPKs such as JNK, p38, and Erk1/2, as well as NF-κB, were engaged after TLR4 activation in cultured astrocytes and neurons. We found that LPS exposure did not alter JNK and phosphorylated (p)-JNK levels in astrocytes or neurons in co-cultures (Fig. S4, A–C). LPS significantly increased p38 and p-p38 levels in

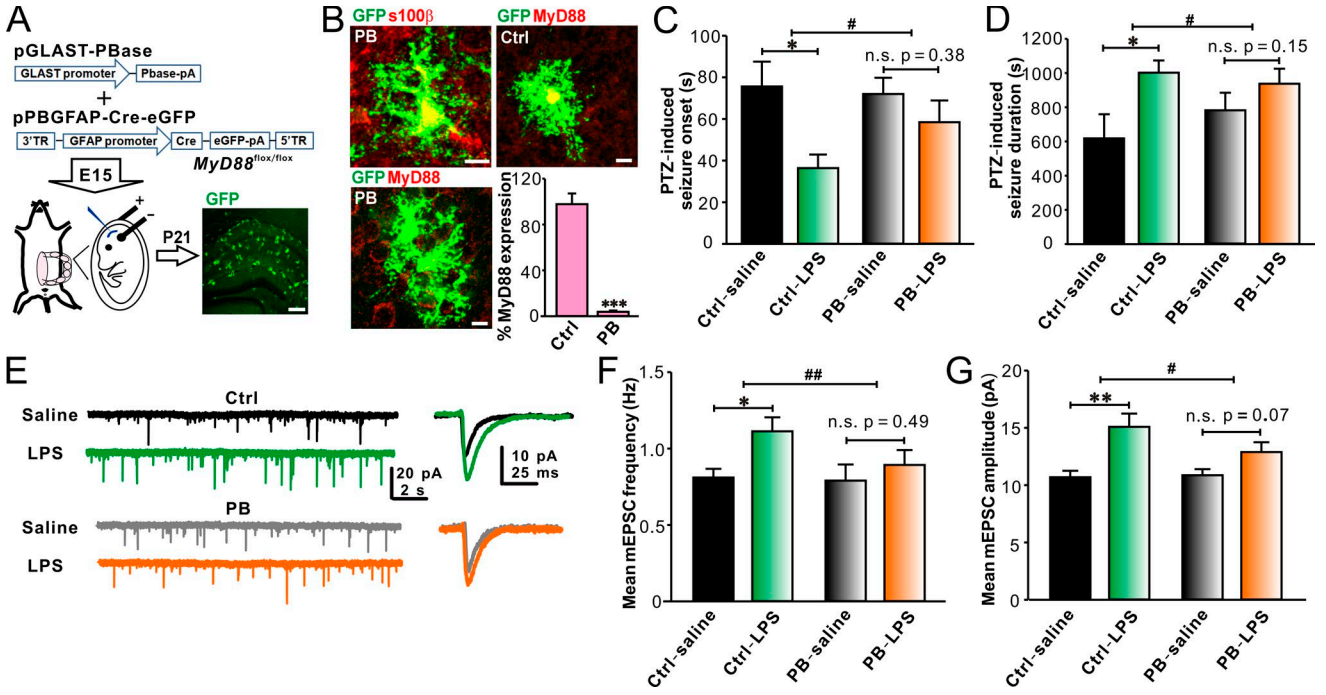


Figure 6. **Astrocytic MyD88 deletion in vivo attenuates the effects of LPS on PTZ-induced seizure susceptibility and excitatory synaptic transmission in juvenile mice.** (A) Schematics of experimental procedures of *piggyBac* (PB)–IUE in *MyD88*$^{flox/flox}$ mice (left) and representative image of hippocampal slices from PB-IUE mice (right). Bar, 200 µm. (B) Representative GFP-positive cells electroporated with the PB (left) and control (Ctrl; top right) plasmids in the hippocampus immunohistostained with s100β (top left) and MyD88 (bottom left and top right) and quantification of the percentage of MyD88 expression in GFP-positive astrocytes (bottom right). *n* = 7 for each group. Bars, 10 µm. Partially deleting astrocytic MyD88 abolished LPS-induced reduction in onset (C) and prolongation of duration (D) of PTZ-induced seizures in young mice. *n* = 6, 5, 6, and 7 for Ctrl-saline, Ctrl-LPS, PB-saline, and PB-LPS groups, respectively. (E) Representative traces of mEPSC recordings in CA1 pyramidal neurons from P14 IUE mice. Astrocytic MyD88 deletion prevented LPS-induced increases in mEPSC frequency (F) and amplitude (G) in CA1 pyramidal neurons from P14 IUE mice. *n* = 6, 7, 9, and 9 for Ctrl-saline, Ctrl-LPS, PB-saline, and PB-LPS groups, respectively. *, P < 0.05; **, P < 0.01; ***, P < 0.001; #, P < 0.05; ##, P < 0.01 (in B, *t* test; in C, D, F, and G, two-way ANOVA with the post hoc Holm-Sidak test). Data are mean ± SEM.

neurons in co-cultures, whereas only increased p-p38 in astrocytes (Fig. S4, D–F). LPS also raised p65 (an NF-κB subunit) and p-p65 levels in neurons in co-cultures, whereas LPS only elevated p-p65 level in astrocytes (Fig. S4, G–I). Notably, LPS specifically increased Erk1/2 and p-Erk1/2 levels in astrocytes rather than in neurons in co-cultures (Fig. 7, A–C). LPS exposure-induced changes in the levels of MAPKs and NF-κB in neurons alone were similar to those in neurons in co-cultures (unpublished data). Moreover, peripheral LPS challenges markedly increased the number of p-Erk1/2–positive astrocytes in the hippocampus of juvenile GFAP-GFP mice (Fig. 7 D), consisting with the result observed in cultured cells. These results indicate that TLR4 activation results in differential activation of downstream signaling mediators in astrocytes and neurons, and Erk1/2 signaling is specifically and significantly enhanced in astrocytes after TLR4 stimulation.

To determine whether Erk1/2 activation is MyD88 dependent, we then examined Erk1/2 levels in *TLR4*$^{-/-}$ or *MyD88*$^{-/-}$ astrocytes, as well as in hippocampal neurons co-cultured with *TLR4*$^{-/-}$ or *MyD88*$^{-/-}$ astrocytes, in response to LPS exposure. Erk1/2 and p-Erk1/2 levels were not significantly altered in astrocytes from *TLR4*$^{-/-}$ or *MyD88*$^{-/-}$ mice and neurons co-cultured with *TLR4*$^{-/-}$ or *MyD88*$^{-/-}$ astrocytes (Fig. 7, E–J), supporting that astrocytic Erk1/2 activation is specifically involved in LPS-induced signal transduction.

Does astrocytic activation of Erk1/2 during postnatal development is sufficient and necessary to promote synaptogenesis and dendritic branching? To address this question, we first transfected the cultured astrocytes with a vector (pXJ40-MYC) that expresses a constitutively active Src homology 2 domain-containing phosphotyrosine phosphatase 2 (SHP2) mutant (SHP2$^{E76V}$; see details in the Materials and methods), which relieves its autoinhibition and constitutively activates Erk1/2 (Li et al., 2014). The transfection rate in astrocytes was ∼70.3 ± 15.6%, and Erk1/2 expression in SHP2$^{E76V}$-transfected astrocytes was 1.60 ± 0.19 relative to that in astrocytes transfected with an empty vector (Fig. 8 A). ACM from SHP2$^{E76V}$-transfected astrocytes significantly raised the densities of PSD95 puncta (Fig. 8, B and C) and synaptophysin/PSD95 colocalized puncta (Fig. 8, B and D) in cultured hippocampal neurons. However, ACM from SHP2$^{E76V}$-transfected astrocytes only slightly increased the dendritic length, whereas it had no effect on the dendritic number of cultured hippocampal neurons (Fig. 8, E and F). These results indicate that constitutively activating Erk1/2 in astrocytes is sufficient to promote synaptogenesis in cultured hippocampal neurons, whereas astrocytic Erk1/2 up-regulation only slightly changes the dendritic pattern in neurons.

Next, we determined to investigate whether TLR4–MyD88 signaling was required for constitutively active Erk1/2 to promote synaptogenesis. We transfected *MyD88*$^{-/-}$ astrocytes with SHP2$^{E76V}$ and then applied ACM from SHP2$^{E76V}$-transfected *MyD88*$^{-/-}$ astrocytes to primary hippocampal neuron cultures. ACM from SHP2$^{E76V}$-transfected *MyD88*$^{-/-}$ astrocytes was able to significantly increase the densities of PSD95 puncta (Fig. 8 G) and synaptophysin/PSD95 colocalized puncta

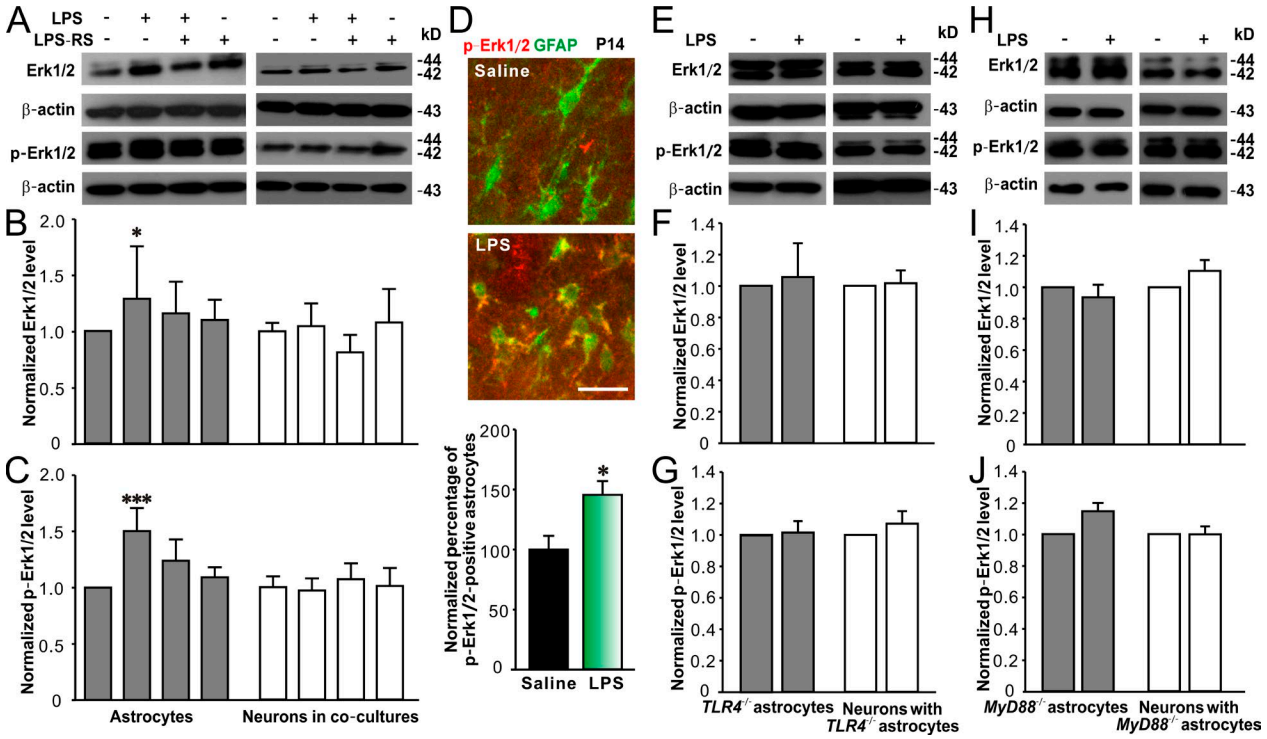


Figure 7. **LPS-activated TLR4–MyD88 signaling pathway in astrocytes involves Erk1/2 activation.** Representative Western blots of Erk1/2 and p-Erk1/2 from cultured astrocytes and hippocampal neurons (DIV15) in co-cultures (A) and quantification of Erk1/2 (B) and p-Erk1/2 (C) expression showing LPS significantly increased Erk1/2 and p-Erk1/2 levels in astrocytes. $n = 4$ for each group. (D) Representative images (top) of immunohistostaining of colocalization of p-Erk1/2 (red) in hippocampal CA1 area of P14 GFAP-GFP mice treated with saline or LPS and quantification of the percentage of p-Erk1/2–positive astrocytes (bottom). Bar, 25 µm. $n = 11$ for each group. Representative Western blots of Erk1/2 and p-Erk1/2 from cultured *TLR4*$^{-/-}$ astrocytes and neurons co-cultured with *TLR4*$^{-/-}$ astrocytes (E) and quantification of Erk1/2 (F) and p-Erk1/2 (G). $n = 4$ for each group. Representative Western blots of Erk1/2 and p-Erk1/2 from cultured *MyD88*$^{-/-}$ astrocytes and neurons co-cultured with *MyD88*$^{-/-}$ astrocytes (H) and quantification of Erk1/2 (I) and p-Erk1/2 (J). $n = 3$ for each group. β-Actin is shown as a loading control. *, $P < 0.05$; ***, $P < 0.001$ (in B and C, one-way ANOVA with the post hoc Dunnett's test; in D, *t* test). Data are mean ± SEM.

(Fig. 8 H) in cultured hippocampal neurons, and these increments of puncta densities could be blocked by MAPK kinase (MEK) 1/2 inhibitor U0126 (Fig. 8, G and H). The results illustrate that Erk1/2 activation alone is sufficient to up-regulate synaptogenesis in cultured hippocampal neurons.

Finally, we tested whether blocking Erk1/2 would rescue LPS-induced synapse abnormalities and seizure susceptibility. We designed specific shRNAs to knockdown Erk1/2 in astrocytes (see details in the Materials and methods) and then added A/LPS from astrocytes transfected with Erk1-shRNA or Erk2-shRNA to hippocampal neuron cultures. The shRNAs reduced Erk1 and Erk2 levels in astrocytes by ~60% (Erk1-shRNA) and 40%, respectively (Erk2-shRNA; Fig. 9 A). Compared with A/LPS from astrocytes transfected with negative ctrl-shRNA, A/LPS from astrocytes transfected with Erk1-shRNA or Erk2-shRNA had less effect on synaptogenesis (Fig. 9, B–D) in cultured hippocampal neurons. MEK1/2 inhibitor U0126 (20 µM) also suppressed the effect of LPS on synaptogenesis in hippocampal neurons co-cultured with astrocytes (Fig. 9, E–G). Furthermore, i.p. injection of MEK1/2 inhibitor SL327 (32 mg/kg) significantly attenuated LPS-induced reduction of the onset (Fig. 9 H) and prolonged the duration (Fig. 9 I) of PTZ-induced seizures in WT mice, indicating that Erk1/2 activation is important for LPS-induced enhancement of seizure susceptibility in the second postnatal week. Collectively, these results indicate that LPS regulation on synapse development and seizure sensitivity is mediated by Erk1/2 activation in astrocytes.

## Discussion

These results demonstrate a major function of astrocyte during early postnatal development and unravel a key TLR4-mediated pathway in astrocytes regulating postnatal excitatory synapse development. Astrocytic activation of TLR4–MyD88–Erk1/2 pathway promoted excitatory synapse generation in the second postnatal week in mice. Immune activation during this critical time period thus causes a marked increase of excitatory synaptic transmission in hippocampus. As the hippocampus initiates and spreads seizure activities, the findings could have direct relevance for the cause of childhood seizures and epilepsy.

In the present study, we used a systemic LPS treatment method to induce a predisposition to seizure generation in young mice. Peripheral infections are commonly associated with sickness behaviors, implicating that systemic inflammation may cause central effects (Simard and Rivest, 2005). Epidemiological studies have shown that systemic inflammatory diseases are often found in patients with epilepsy (Téllez-Zenteno et al., 2005). In experimental models, peripheral inflammation can lower seizure threshold, and this increased seizure susceptibility might be because of a "mirror" CNS inflammatory response caused by peripheral infectious agents (Riazi et al., 2010). Although we do not know whether our systemic treatment of LPS elicits the profound central consequence via a direct effect of circulating LPS (Chakravarty and Herkenham, 2005; Rivest, 2009) or a secondary effect of LPS-induced

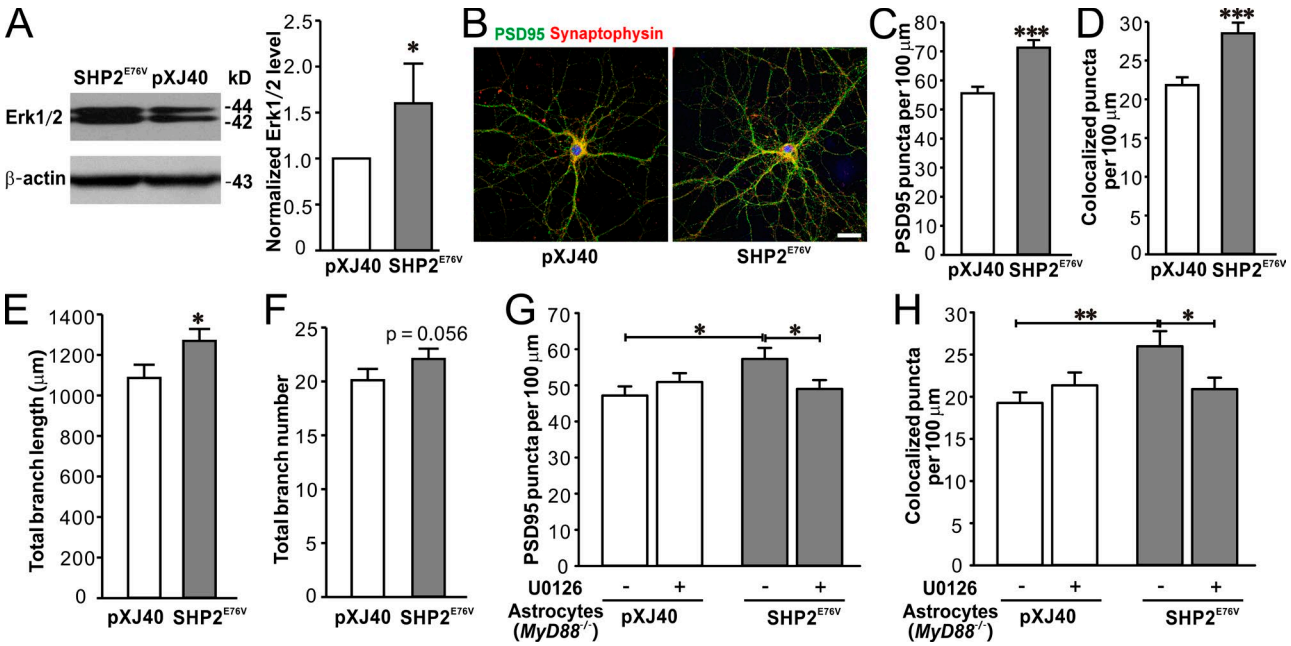


Figure 8. **Erk1/2 activation in astrocyte is sufficient for LPS-induced promotion of synapse development in neurons co-cultured with astrocytes.** (A) Representative Western blots of Erk1/2 (left) from cultured astrocytes transfected with SHP2$^{E76V}$ and pXJ40-myc (pXJ40; empty vector) and quantification of Erk1/2 expression (right) showing up-regulated Erk1/2 in SHP2$^{E76V}$-transfected astrocytes. *n* = 4 for each group. (B) Representative images of immunostaining of PSD95 (green), synaptophysin (red), and DAPI (blue) in neurons treated with ACM from astrocytes transfected with pXJ40 (left) or SHP2$^{E76V}$ (right). Bar, 25 µm. Quantification of PSD95 puncta (C) and PSD95/synaptophysin colocalized puncta (D) in neurons treated with ACM from astrocytes transfected with pXJ40 or SHP2$^{E76V}$. *n* = 29 and 33 for pXJ40 and SHP2$^{E76V}$ groups, respectively. Quantification of the length (E) and number (F) of dendritic branching in neurons treated with ACM from astrocytes transfected with pXJ40 or SHP2$^{E76V}$. *n* = 29 and 33 for pXJ40 and SHP2$^{E76V}$ groups, respectively. Quantification of PSD95 puncta (G) and PSD95/synaptophysin colocalized puncta (H) in neurons treated with ACM from *MyD88*$^{-/-}$ astrocytes transfected with pXJ40 or SHP2$^{E76V}$, with or without U0126, an MEK1/2 inhibitor. *n* = 31 and 32 for pXJ40- and SHP2$^{E76V}$-groups, respectively. *, P < 0.05; **, P < 0.01; ***, P < 0.001 (in A and C–E, *t* test; in G and H, two-way ANOVA with the post hoc Holm-Sidak test). Data are mean ± SEM.

peripheral inflammatory mediators, both may contribute to the increased astrocyte activation and astrocytic TLR4 activation in young mice (Fig. 2). It will be interesting to determine if circulating LPS can be directly recognized by CNS-resident cells including parenchymal glial cells in future studies.

Our results showed that systemic LPS treatment induced astrocyte activation in young mice, whereas it did not affect microglia activation. This could be because of the fact that we used a relatively low-dose LPS to challenge the juvenile mice. Similar results were observed in young rats treated with low-dose LPS (Galic et al., 2008). In addition, whereas microglia are the main immunocompetent cells in the immature brain, LPS may predominantly bind TLR4 in astrocytes in the neonate brain (Sherwin and Fern, 2005). Interestingly, resting microglia express considerably more TLR4 than do resting astrocytes (Lehnardt et al., 2002). Future studies are required to clarify whether TLR4 level is up-regulated in reactive astrocytes upon TLR4 stimulation in the developing brain (Jack et al., 2005).

Astrocyte-mediated signaling events are critical in wiring and shaping the neural circuits. We showed that activating TLR4 in astrocytes facilitated excitatory synapse generation in the second postnatal week. At early developmental stages, astrocytes are well known to contribute to normal synapse development. Many important molecules are released from astrocytes during early development, promoting synapstogenesis in adjacent neurons. For example, astrocyte-derived thrombospondings (TSPs) help to form structurally stable excitatory synapses (Christopherson et al., 2005; Eroglu et al., 2009); astrocyte-derived glypicans further help to incorporate glutamate receptors into the postsynaptic site, forming functional synapses (Allen et al., 2012). Interestingly, LPS treatments at P10–12 rapidly increased synaptogenesis in the hippocampus of p14 mice (Fig. 1). This is not surprising because astrocyte-mediated promotion of synapse formation is generally fast. For instance, it takes 3–6 d for TSPs to have significant prosynaptogenic effects (Christopherson et al., 2005; Xu et al., 2010). Our results revealed that in the second postnatal week, astrocytes are indispensable in response to pathological insults by means of regulating synapse formation. Maturing astrocytes monitor the surrounding environment, recognize pathogen-associated molecular patterns and damage-associated molecular patterns via their surface TLRs, and respond with an increased synaptogenesis possibly because of a compensatory purpose. Thus, maturing astrocytes are critical in the temporal control of brain wiring under both physiological and pathological conditions.

Cumulating evidence supports ERK signaling as crucial for balancing neurogenesis and astrogenesis during embryonic and early postnatal development. Activating the SHP2–Ras–Raf–MEK–ERK pathway in nonneuronal cells inhibits astrogenic Janus kinase–signal transducer and activator of transcription 3 signaling and promotes neurogenesis (Xu and Qu, 2008). Sustained SHP2 activation thus results in an increased neuron to astrocyte ratio (Gauthier et al., 2007), which may impede astrocyte-regulated synapse development. However, this suppression of synapse formation by decreased number of astrocytes may be counteracted by ERK activation in astrocytes, as our data clearly show that ERK activation in astrocytes promotes synaptogenesis. This may explain why excitatory synapse

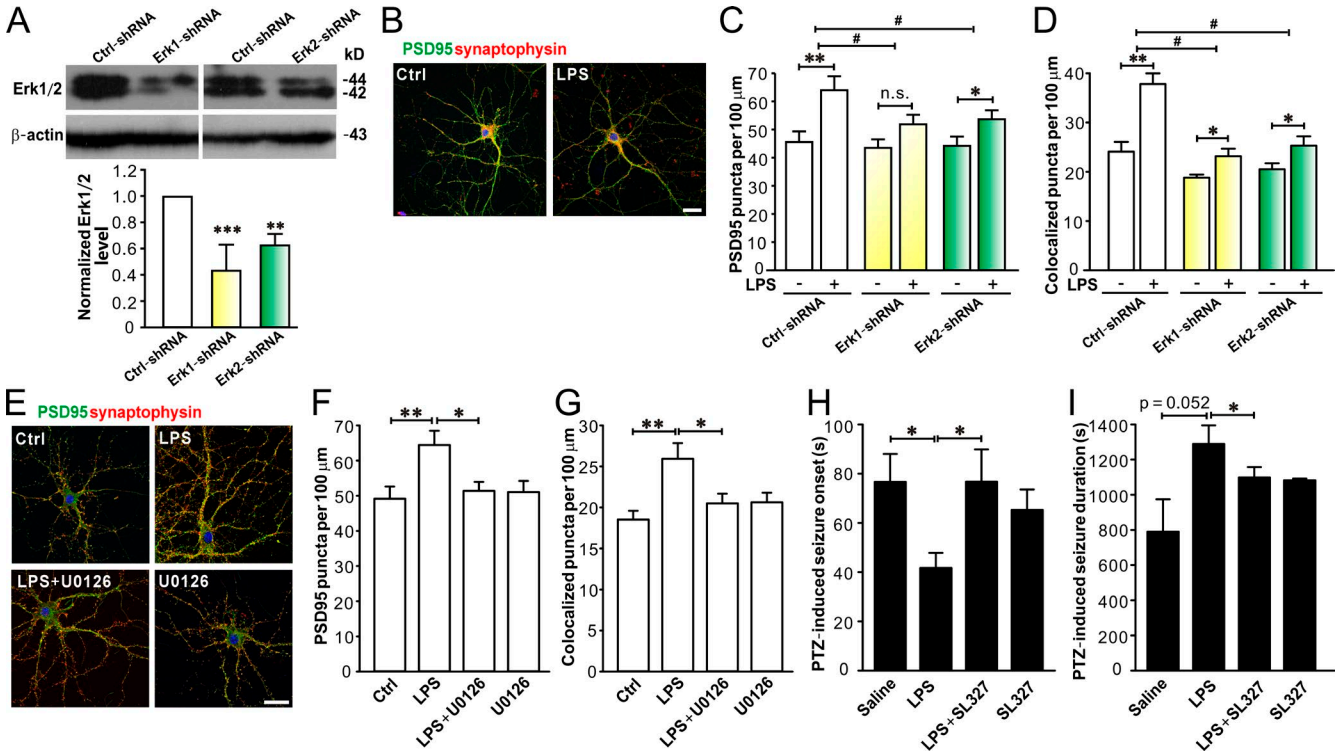


Figure 9. **Erk1/2 activation in astrocytes is necessary for LPS-induced effects on synapse development and PTZ-induced seizure susceptibility.** (A) Representative Western blots of Erk1/2 (top) in astrocytes transfected with ctrl-shRNA, Erk1-shRNA, or Erk2-shRNA, and quantification of Erk1/2 expression (bottom). *n* = 4, 4, and 3 in ctrl-shRNA, Erk1-shRNA, and Erk2-shRNA groups, respectively. (B) Representative images of immunostaining of PSD95 (green), synaptophysin (red), and DAPI (blue) in cultured neurons treated with ACM from Erk1-shRNA knockdown astrocytes exposed to vehicle (Ctrl) or LPS. Bar, 25 µm. Quantification of PSD95 puncta (C) and PSD95/synaptophysin colocalized puncta (D) in neurons treated with ACM from astrocytes transfected with ctrl-shRNA, Erk1-shRNA, or Erk2-shRNA (exposed to vehicle or LPS). *n* = 27, 29, and 30 in ctrl-shRNA, Erk1-shRNA, and Erk2-shRNA groups, respectively. (E) Representative images of hippocampal neurons co-cultured with astrocytes exposed to vehicle (Ctrl), LPS, LPS + U0126, or U0126. Bar, 25 µm. Quantification of PSD95 puncta (F) and PSD95/synaptophysin colocalized puncta (G) in co-cultured neurons from E. *n* = 27, 29, 28, and 29 in Ctrl, LPS, LPS+U0126, and U0126 groups, respectively. MEK1/2 inhibitor SL327 attenuated LPS-induced reduction in onset (H) and prolongation of duration (I) of PTZ-induced seizures in young mice. *n* = 5, 5, 6, and 5 for Ctrl, LPS, LPS+SL327, and SL327 groups, respectively. *, $P < 0.05$; **, $P < 0.01$; ***, $P < 0.001$; #, $P < 0.05$ (in A and F–I, one-way ANOVA with the post hoc Dunnett's test; in C and D, two-way ANOVA with the post hoc Holm-Sidak test). Data are mean ± SEM.

number is actually increased in a mouse model of Noonan syndrome expressing a constitutively active SHP2 (Lee et al., 2014). The other route of MEK/ERK activation in astrocytes is via TLR stimulation in a MyD88-dependent manner. Although we do not know the identity of the MAPK kinase kinase in this pathway, MAPK kinase kinases such as TGF-β–activated kinase 1 (Goldmann et al., 2013) and tumor progression locus 2 (Hirschhorn et al., 2014) are known to be present in glial cells. As a converging point of Ras- and TLR-mediated prosynaptogenic pathways, ERK bridges innate immune reactions and neurotrophic factor–induced effects.

Some of our key results were obtained from the noncontact astrocyte-neuron co-culture and ACM-treated neuronal culture experiments, suggesting a secreted molecule from astrocytes may mediate abnormal excitatory synapse development in response to Erk1/2 activation. As mentioned above, maturing astrocytes secrete a variety of factors that facilitate normal synaptogenesis during postnatal development. It is possible astrocytic ERK activation augments synapse formation by merely increasing the amount of these secreted molecules. Although we do not know the identity of the secreted molecule yet, it is unlikely TSP1 release is increased upon TLR4 activation, as previous studies have shown that ERK phosphorylation leads to a decrease in TSP1 transcription (Chen et al., 2011) and translation (Ikeda et al., 2010) in astrocytes. Detailed screening is ongoing to uncover the molecule(s) released from astrocytes in response to TLR4 stimulation.

Our results indicate that the prosynaptogenic effect of astrocytic TLR4 activation is profound in the second postnatal week and quickly subsidized in the following weeks in mice. This decline is probably not because of a down-regulation of key factors in the TLR4–ERK pathway, as TLR4, MyD88, and Erk1/2 are all expressed in mature astrocytes. Innate immune responses are often controlled by negative regulators, because excessive and unleashed responses are extremely harmful and can cause severe inflammatory diseases such as septic shock and chronic inflammation. Thus, it is possible some key negative regulators of TLR4–ERK signaling are up-regulated with postnatal development in astrocytes. Negative regulators of TLR–ERK signaling, such as receptor tyrosine kinase adaptors downstream of kinases 1 and 2, are present in microglia and astrocytes (Downer et al., 2013). It will be interesting to test their involvement in controlling TLR4–ERK signaling in the developing astrocytes in future studies. Alternatively, some unknown factors downstream to the TLR4–ERK pathway may be developmentally regulated. Secreted molecules from astrocytes and their signaling partners in neurons may well be subjected to postnatal regulation.

In conclusion, the current work depicts a crucial TLR4-mediated pathway in astrocytes underpinning peripheral immune challenge-induced seizure susceptibility during postnatal development. This signaling pathway may also be relevant to CNS infection–induced seizures and epilepsy in children. Most infectious agents associated with childhood seizures and epilepsy are recognized by TLRs in a MyD88-dependent manner. Therefore, the MyD88-dependent Erk1/2 activation may serve as a common pathological mechanism for many immune activation–related diseases.

## Materials and methods

### Animals

All procedures were performed in accordance with the National Institutes of Health Guidelines for the Care and Use of Laboratory Animals and approved by the Animal Advisory Committee at Zhejiang University. B6 (stock number 000664), *TLR4*$^{-/-}$ (C57BL/10ScNJ; stock number 003752), *MyD88*$^{-/-}$ [B6.129P2(SJL)-*Myd88tm1.1Defr/J*; stock number 009088], *MyD88*$^{flox/flox}$ [C57BL/6-Tg(Camk2a-ESR1/Disc1*)2698.1Sva/J; stock number 008088], and GFAP-GFP [D2.FVB-Tg(GFAPGFP)14Mes/SjJ; stock number 026856] mice were purchased from The Jackson Laboratory. All mice were housed at the Animal Facility of Zhejiang University under a 12-h light/dark cycle and had access to food and water ad libitum. In total, ∼191 mice were used in this study. Pregnant mice were used for primary neuron cultures and IUE. For behavioral experiments, only male mice were used.

### PTZ-induced seizure test

PTZ dose used in this study (40 mg/kg in young mice and 50 mg/kg in adult mice, in 0.9% saline, i.p. injection volume was 1 ml/100 g body weight) was determined as a dose at which PTZ induced seizures in 75% of naive mice. In brief, 2- and 11-wk-old mice treated with drugs (saline, LPS [1.0 mg/kg/d; Sigma-Aldrich], SL327 [selective inhibitor MEK1 and MEK2; 32 mg/kg/d; Tocris Bioscience], or LPS plus SL327, i.p. injection for 3 d [P10–12 or P70–72; see details in the figure legends]) were individually placed in a Plexiglas box, and convulsive behaviors were analyzed for 30 min after PTZ injection. The time to onset and the duration of tonic-clonic seizures were measured as previously described (Shen et al., 2012).

### Golgi staining

Golgi stainings were performed using a Rapid GolgiStain Kit (PK401; FD Neurotechnologies, Inc.) according to the manufacturer's instructions (Ramanan et al., 2005). In brief, nonperfused mouse brains were immersed in impregnation solution for 2 wk and then transferred to Solution C for 2 d. Sections of 200-µm thickness were serially cut with a freezing microtome (CM30503; Leica Biosystems). Sections were mounted on 3% gelatin-coated slides and allowed to dry for 2 wk before being stained with silver nitrate solution Solution D and E, dehydrated through descending alcohol series, and mounted with Permount (Thermo Fisher Scientific). Images were acquired with a microscope (BX53; Olympus) at room temperature, and neuronal morphology analysis was performed using ImageJ software (National Institutes of Health). At least five pyramidal neurons in the hippocampal CA1 region per mouse were randomly selected. Neurons were then reconstructed by a researcher who was blinded to the identity of each group using a camera lucida and a 40× objective (NA 0.95). Dendritic length was calculated for each neuron reconstructed. In brief, concentric spheres of increasing radius (10-µm increments) were placed around the center of the cell body until dendrites were completely captured. The number of dendritic intersections was counted and expressed as total number of intersections starting at the center of the soma. The density of dendritic spines of a distinct branch was measured by a 100× oil-immersion objective (NA 1.3). Spines visible along both sides of dendritic segments were counted and expressed as mean number of spines per micrometer (Sholl, 1953). Two-way analysis of variance (ANOVA) followed by a post hoc multiple comparison analysis based on the Holm-Sidak method were used to determine significant levels between the saline and LPS groups.

### Slice recording

Mice (2 or 10 wk old) were anesthetized with isoflurane and the brain was then removed after decapitation. The brain areas containing hippocampus were dissected rapidly and transferred to a chamber filled with ice-cold artificial cerebrospinal fluid (ACSF; 124 mM NaCl, 2 mM KCl, 1.25 mM $KH_2PO_4$, 2 mM $MgSO_4$, 2 mM $CaCl_2$, 26 mM $NaHCO_3$, and 10 mM D-glucose, pH 7.4, 300 mosM). Transverse hippocampal slices (300 µm) were cut with a tissue slicer (VT 1200S; Leica Biosystems) and incubated in oxygenated (95% $O_2$/5% $CO_2$) ACSF. Slices were allowed to recover for ∼30 min in ACSF at 32°C and subsequently for 1 h at room temperature. Hippocampal slices were then transferred to a recording chamber and perfused continuously with ACSF at 35°C bubbled with 95% $O_2$/5% $CO_2$ to ensure adequate oxygenation of slices. Whole-cell recordings were performed on CA1 pyramidal neurons. Neurons were identified under infrared differential interference contrast optics based on their location and morphology. Borosilicate glass pipettes (3–6 MΩ; A-M Systems) were pulled with a horizontal pipette puller (P97; Sutter Instrument) and filled with artificial intracellular fluid (120 mM potassium gluconate, 15 mM KCl, 10 mM Hepes, 4 mM Mg-ATP, 0.3 mM Tris-GTP, and 0.5 mM EGTA, pH 7.3, 285–290 mosM). Pipettes were connected to the headstage of an EPC 10 amplifier (HEKA), and fast and slow capacitance as well as series resistance compensations were carefully adjusted. Liquid junction potentials were not corrected. mEPSCs were recorded at −70 mV in ACSF containing 0.5 µM tetrodotoxin (TTX; Ascent Scientific) and 10 µM bicuculline (Ascent Scientific). Series resistance was normally <20 MΩ, and recordings of >20% change in series resistance were terminated and discarded. Electrophysiological recordings were filtered at 2.0 kHz and digitized at 50 kHz. All reagents were purchased from Sigma-Aldrich unless otherwise specified. Individual events were counted and analyzed with Mini Analysis (Synaptosoft). For kinetic analysis, only single-event mEPSCs with a stable baseline, sharp rising phase (10 to 90% rise time), and exponential decay were chosen during visual inspection of the recording traces. Double- and multiple-peak mEPSCs were excluded. 300 s of recordings randomly chosen from five cells in each group were analyzed (Zhou et al., 2009; Shen et al., 2012).

### Immunohistochemistry

Mice were deeply anesthetized with isoflurane and perfused transcardially with 4% PFA in PBS. Brains were extracted and postfixed in 4% PFA overnight and then moved to 30% sucrose in PBS. After brains were saturated (36 h), coronal brain sections (30-µm thickness) were cut using a freezing microtome (CM30503; Leica Biosystems). Sections were processed as free-floating sections. After being blocked in PBS containing 5% normal donkey serum (NDS; 017-000-121; Jackson ImmunoResearch Laboratories, Inc.), 1% BSA (Sigma-Aldrich), and 0.3% Triton X-100 (Sigma-Aldrich) for 1 h at room temperature, tissue sections were incubated with primary antibodies (rabbit anti–GFAP [1:1,000; Z0334; Dako], rabbit anti–Iba-1 [1:500; 019-19741; Wako Pure Chemical Industries], mouse anti–TLR4 [1:200; sc-293072; Santa Cruz Biotechnology, Inc.], rabbit anti–MyD88 [1:50; ab2068; Abcam], rabbit anti–phosphorylated (p)-Erk1/2 [1:50; 4370; Cell

Signaling Technology], and mouse anti–s100β [1:1,000; SAB4200671; Sigma-Aldrich]) overnight at 4°C in the blocking solution. Tissue sections were washed in PBS (15 min, three times), incubated with an appropriate secondary antibody (Alexa Fluor 488 anti–mouse IgG [1:1,000; A-21202; Thermo Fisher Scientific] or Alexa Fluor 546 anti–rabbit IgG [1:1,000; A10040; Thermo Fisher Scientific]) for 1 h at room temperature. After being washed with PBS three times, sections were mounted onto glass slides with ProLong Gold Antifade Reagent (P36931; Thermo Fisher Scientific). Images were captured using an A1 laser-scanning confocal microscope through a 20× objective (NA 0.75; Nikon) and taken at a resolution of 1,024 × 1,024 pixels at room temperature under a fixed set of settings. Fluorescence intensities and cell numbers were analyzed by MetaMorph (Molecular Devices) with a fixed set of parameters.

### Cell cultures and drug treatments

Hippocampal neurons from embryonic day 18 (E18) mice were prepared as described previously (Zhang et al., 2010; Shen et al., 2011). In brief, embryos were removed from maternal mice anesthetized with isoflurane and euthanized by decapitation. Hippocampi were dissected and placed in $Ca^{2+}$- and $Mg^{2+}$-free Hepes-buffered HBSS, pH 7.45, followed by a digestion with 0.25% wt/vol trypsin. After trituration through a Pasteur pipette, neurons were centrifuged (1,000 *g* for 5 min) and resuspended in Neurobasal medium containing 2% B27 serum-free supplement, 1% vol/vol penicillin/streptomycin, 0.5 mM glutamine, and 10 µM glutamate (Sigma-Aldrich). Dissociated cells were then plated at a density of $0.03 \times 10^6$ cells/cm$^2$ onto 12-mm round coverslips in 24-well plates (for immunochemistry and recording) or at a density of $0.05 \times 10^6$ cells/cm$^2$ in 6-well plates (for Western blots) precoated with poly-D-lysine (50 µg/ml; Sigma-Aldrich). Cultures were kept at 37°C in a 5% vol/vol $CO_2$-humidified incubator. Thereafter, one third to half of the medium was replaced twice a week with Neurobasal culture medium containing 2% B27 supplement and 0.5 mM glutamine. Cultured astrocytes were prepared as described previously with minor modifications (McCarthy and de Vellis, 1980; Foo et al., 2011). Cortices were dissected from 0- to 1-d-old mice (P0 to -1; WT, *TLR4*$^{-/-}$, and *MyD88*$^{-/-}$) and digested with 0.25% wt/vol trypsin in DMEM. Tissue was triturated and resuspended after centrifugation in astrocyte culture medium (DMEM containing 10% vol/vol FBS and 1% vol/vol penicillin/streptomycin). Cells were plated in T-75 flasks at the density of two cortices per flask (Costar; Corning) precoated with poly-D-lysine. The cells were grown for at least 7 d at 37°C with 5% vol/vol $CO_2$, and a complete medium change was performed every other day. At confluence after DIV8–10, cultures were shaken for 12–16 h at 250 rpm at 37°C on an orbital shaker (KS4000i Control Incubating Shaker; IKA) followed by an incubation in culture medium containing 20 µM cytosine-1-β-D-arabinofuranosid (Sigma-Aldrich) for 2 to 3 d to deplete the precursor cells and to achieve a confluent layer of astrocytes. Purified astrocyte cultures contained very little microglia, as estimated by immunofluorescence (with rabbit anti–Iba-1 [1:500; 019-19741; Wako] and rabbit anti–GFAP antibody [1:1,000; Z0334; Dako]) and Western blots. The percentage of Iba-1–positive cells in the astrocyte cultures was 5.6 ± 0.4% ($n$ = 10 fields from three cultures, using 20× objective), and Iba-1 expression was 6.9 ± 0.7% of GFAP expression in astrocyte cultures. For co-culture experiments, neurons and astrocytes were cultured in an indirect co-culture assay with or without direct contacts, but sharing the same defined medium (Pyka et al., 2011). In brief, astrocytes were subcultured in cell culture inserts (Transwell inserts, pore size 0.4 µm; BD) at a density of 25,000 cells per insert via enzymatic digestion with 0.05% wt/vol trypsin with EDTA. After an adherence time of 48 h, the transwell inserts with astrocytes were placed into six-well plates with hippocampal neurons at DIV4 to 5, and the astrocyte medium was replaced with the neuron medium. In experiments dealing with ACM, ACM was collected 4 to 5 d after replacing the astrocyte culture medium with the neuron culture medium. Neurons at DIV4 to 5 were cultured with ACM, and half of the medium was replaced at DIV8 with fresh ACM. At DIV13, half of the medium was replaced with ACM collected from astrocytes treated with LPS or vehicle. At 48 h before immunocytochemistry experiments were performed, TLR4 agonist LPS (1 µg/ml; Sigma-Aldrich), antagonist LPS-RS (10 µg/ml; InvivoGen), and/or MEK1/2 inhibitor U0126 (20 µM; EMD Millipore) were added into the culture media for neuron cultures and astrocyte-neurons co-cultures. Propidium iodide (Sigma-Aldrich) staining was used to detect the cell survival rate. For ACM experiments, at 48 h before ACM collection, LPS was added in astrocyte cultures. All reagents were purchased from Thermo Fisher Scientific unless otherwise specified.

### Cultured neuron recording

Immediately before electrophysiological recording, neurons at DIV15 were transferred to a perfusion chamber and visualized with an inverted microscope (IX51; Olympus). Whole-cell patch-clamp recordings were performed in the voltage-clamp mode at room temperatures (22–23°C) at a holding potential of −70 mV. For mEPSC recordings, neurons were perfused with a bath solution containing 145 mM NaCl, 5 mM KCl, 2 mM $CaCl_2$, 2 mM $MgCl_2$, 10 mM glucose, and 10 mM Hepes, pH 7.40 (290–310 mosM), and mEPSCs were pharmacologically isolated by adding 0.5 µM TTX and 10 µM bicuculline to the bath solution. Patch pipettes (4–6 MΩ) were filled with artificial intracellular fluid: 140 mM potassium gluconate, 10 mM KCl, 5 mM NaCl, 2 mM $MgCl_2$, 1 mM $CaCl_2$, 5 mM EGTA, 5 mM Hepes, and 3 mM ATP, pH 7.30 (290–300 mosM). For mIPSC recordings, neurons were perfused with a bath solution containing: 137 mM NaCl, 5 mM KCl, 2 mM $CaCl_2$, 1 mM $MgCl_2$, 20 mM glucose, and 10 mM Hepes, pH 7.40 (310–320 mosM), and mIPSCs were pharmacologically isolated by adding 0.5 µM TTX, 40 µM APV (Ascent Scientific), 10 µM CNQX (Ascent Scientific), and 1 µM CGP54626 (Tocris Bioscience) to the bath solution. Patch pipettes (4–6 MΩ) were filled with artificial intracellular fluid: 137 mM CsCl, 2 mM $MgCl_2$, 1 mM $CaCl_2$, 11 mM EGTA, 10 mM Hepes, and 3 mM ATP (pH 7.30, 290–300 mosM). All reagents were purchased from Sigma-Aldrich unless otherwise specified. Recordings were amplified using an Axopatch 200B amplifier (Molecular Devices). Individual events were counted and analyzed with MiniAnalysis as mentioned in the Slice recording section (Shen et al., 2011).

### Immunocytochemistry

Immunocytochemistry experiments were performed as previously described (Xu et al., 2010). In brief, cells on coverslips were fixed by 4% PFA plus 4% sucrose in PBS for 20 min and permeabilized by 0.2% Triton X-100 for 10 min. The cells were blocked with 10% NDS for at least 2 h and then were incubated with primary antibodies (mouse anti-PSD95 [1:500; MAB1596; EMD Millipore] and rabbit anti–synaptophysin [1:500; ab14692; Abcam] or mouse anti–MAP2 [1:1,000; ab7756; Abcam]) diluted in 3% NDS for 1 h. After being washed with PBS for three times, fluorescent secondary antibodies (Alexa Fluor 488 anti–mouse IgG and Alexa Fluor 546 anti–rabbit IgG) were added for 1 h. After being washed with PBS for three times, the coverslips were mounted with ProLong Gold Antifade Reagent for subsequent fluorescent image acquisition. Fluorescent images were acquired using a confocal laser-scanning microscope (LSM510 meta; ZEISS). Pictures were viewed through a 63× oil-immersion objective (NA 1.4) and taken at a resolution of 1,024 × 1,024 pixels at room temperature. An overlay of the single pictures (stacks) was made. Gain, threshold, and black levels were not subjected to change during individual experiments. Neuronal images were analyzed using MetaMorph with customized filter

sets. Images were initially acquired as 12-bit grayscale pictures and prepared for presentation using Photoshop (Adobe Systems). All image analysis was done blind to the experimental condition. Spines were defined as dendritic protrusions of 0.5–3 µm length, with or without a head. The number of excitatory synapses was measured by counting the number of PSD95 puncta in contact with synaptophysin puncta in neurons (~200 µm total dendritic length per neuron; Jaworski et al., 2009). Colocalization of two fluorescent signals was determined using the "colocalization" module in MetaMorph as described (Lee et al., 2004). The colocalization module provides intensity measurements of the region overlap between signals in red and green channels of image projections. To minimize random overlap as a result of projection of confocal images, a single optical section from the z series stack that showed the largest amount of fluorescent signals was used to determine the degree of colocalization in the cell body. Means from multiple individual neurons were averaged to obtain a population mean and SEM. The numbers (*n*) in figure legends represent cell numbers from three to four independent experiments.

### Western blotting

Hippocampi were obtained and homogenized using a chilled Vibra-homogenizer (Vibra-Cell; Sonics and Materials, Inc.) containing 2 ml RIPA buffer (1% Triton X-100, 0.1% SDS, 150 mM NaCl, 2 mM EDTA, 50 mM NaF, 10 mM sodium pyrophosphate, 1.0 mM $Na_3VO_4$, 1.0 mM PMSF, and complete protease inhibitor cocktail; Roche). Cultured neurons and astrocytes were washed twice with ice-cold PBS after the medium was carefully aspirated and then were collected on ice with ice-cold RIPA buffer mentioned above. The lysate was then centrifuged at 14,000 *g* for 15 min at 4°C and the supernatant collected for Western blot analysis. The protein concentration of the probes was determined using a Pierce BCA Protein Assay Kit (Thermo Fisher Scientific), and the tubes were stored at −20°C. 10% SDS-PAGE was used to separate protein samples. After electrophoresis, the gels were transferred to polyvinylidene fluoride membranes (EMD Millipore) using a constant voltage of 300 mV for 90 min. The membranes were then blocked in 5% milk in TBST (25 mM Tris-HCl, 150 mM NaCl, and 0.1% Tween 20, pH 7.4) for 30 min at room temperature on a rocker and incubated in the primary antibody overnight on a rocker at 4°C. Primary antibodies were made with 5% milk in TBST solutions (mouse anti–GFAP [1:1,000; ab10062; Abcam]; rabbit anti–Iba-1 [1:500; 019-19741; Wako Pure Chemical Industries]; mouse anti–TLR4 [1:200; ab22048; Abcam]; mouse anti–Erk1/2 [1:1,000; 4696S; Cell Signaling Technology]; rabbit anti–p-Erk1/2 [1:1,000; 9101S; Cell Signaling Technology]; rabbit anti–MyD88 [1:1,000; ab2064; Abcam]; rabbit anti–p38 [1:1,000; 9212; Cell Signaling Technology]; rabbit anti–p-p38 [1:1,000; 4511S; Cell Signaling Technology]; mouse anti–NF-κB p65 [1:500; 6956; Cell Signaling Technology]; rabbit anti–p-NF-κB p65 [1:500; 3033L; Cell Signaling Technology]; rabbit anti–JNK (1:1,000; 9252; Cell Signaling Technology); rabbit anti–p-JNK [1:1,000; 9251S; Cell Signaling Technology]; and mouse anti–β-actin [1:10,000; Sigma-Aldrich A5441]). After primary antibody incubation, the membranes were rinsed three times in TBST before being incubated with anti–mouse HRP-conjugated secondary antibody (1:10,000 in 5% milk in TBST; 31430; Thermo Fisher Scientific) and anti–rabbit HRP-conjugated secondary antibody (1:10,000; 31460; Thermo Fisher Scientific) for 1 h on a rocker at room temperature. After being washed in TBST three times on a rocker at room temperature, protein bands were then visualized using either ECL or ECL-Plus Western blotting detection reagents (Thermo Fisher Scientific). Quantification of the intensity of the protein bands obtained in Western blots was performed using ImageJ software, and results were normalized to the appropriate β-actin bands.

### The *piggyBac* plasmids and IUE

The *piggyBac* plasmids (including the helper plasmid, pGlast-PBase, and the donor plasmid, pPBGFAP-eGFP) were provided by J. LoTurco (University of Connecticut, Storrs, CT; Chen and LoTurco, 2012). To construct a donor plasmid pPBGFAP-Cre-eGFP, the LoxP site in pPBGFAP-eGFP was removed by using a standard PCR method (the primers were: 5′-GGACTAGTCAGGAAGACGGGGTGTTAC AG-3′ [forward] and 5′-GGACTAGTTGCGATTAATAAGTATAAT TTG-3′ [reverse]). Then a Cre sequence was inserted into the EcoRI site (the primers were 5′-CGGAATTCATGTCCAATTTACTGACCG TACACC-3′ [forward] and 5′-CGGAATTCATCGCCATCTTCCAGC AG-3′ [reverse]). pGlast-PBase and pPBGFAP-eGFP plasmids were used as negative controls. IUE aiming hippocampus was performed on E15 mice, as previously described (Bai et al., 2003; Ramos et al., 2006; Navarro-Quiroga et al., 2007; Chen and LoTurco, 2012). In brief, E15 mice were anesthetized with a gas anesthetizer (Matrx VIP 3000; mix ratio 1.5, flow rate 1.0, consuming 1 ml isoflurane per 10 min; Midmark) before surgery. To visualize the electroporating process, plasmids were mixed with 2 mg/ml Fast Green (Sigma-Aldrich). In all conditions, pPBGFAP-Cre-eGFP and pPBGFAP-eGFP were used at the final concentration of 1.5 µg/µl, whereas pGLAST-PBase was used at the final concentration of 3 µg/µl. During surgery, the uterine horns were exposed, and one lateral ventricle of each embryo was pressure injected with 1 to 2 µl plasmid DNA. Injections were made by inserting a pulled glass microelectrode into the lateral ventricle through the uterine wall and embryonic membranes and injecting the content of the microelectrode by pressure pulses delivered with an electroporator (EDIT-TYPE CUY-21; Nepa Gene). A voltage of 40 V was used for electroporation. Antibiotics were administered at a dose of 1 mg/kg s.c. for 1 d after surgery. To estimate the electroporation efficiency, coronal brain sections (30 µm) from IUE mice were cut using a freezing microtome. Tissue sections were incubated with mouse anti–GFAP and Alexa Fluor 546 anti–rabbit IgG and then mounted onto glass slides with ProLong Gold Antifade Reagent for fluorescent image (as mentioned in Immunohistochemistry). The mean IUE transfection rate was 50.1 ± 8.8% ($n$ = 25), ranging from the lowest rate of 35.9% to the highest rate of 71.8%. Data from mice with an IUE transfection rate <30% were excluded.

### Plasmids, shRNAs, and transfection

The constitutively active SHP2 mutant ($SHP2^{E76V}$) plasmid (pXJ40-MYC-SHP2) and empty vector (pXJ40-MYC) were provided by Y. Ke (Zhejiang University School of Medicine, Hangzhou, China; Li et al., 2014). The E76V mutation in SHP2 releases SHP2 from autoinhibition and constitutively activates Erk1/2. All constructs were verified by sequencing (Thermo Fisher Scientific). For Erk1/2 knockdown experiments, specific shRNAs chemically synthesized by GenChem Research were used. Sequences of the shRNA constructs are as follows: negative control-shRNA (5′-TTCTCCGAACGTGTCACGT-3′), mouse Erk1-shRNA (5′-AAGTTCGAGTAGCTATCAA-3′), and mouse Erk2-shRNA (5′-TGAATTGTATCATCAACAT-3′). All constructs were verified by sequencing (Thermo Fisher Scientific). Plasmids and shRNA transfections were performed with Lipofectamine 2000 (11668-019; Thermo Fisher Scientific) in an Opti-MEM medium (31985070; Thermo Fisher Scientific) according to the vendor's protocol. For each transfection, astrocytes in six-well plates were incubated with plasmid DNA (4 µg) or shRNA (3 µg) combined with Lipofectamine 2000 (4 µl). Each transfection was done in triplicate. ACM from $SHP2^{E76V}$- or shRNA-transfected astrocytes treated with LPS for 48 h was added to neuron cultures as mentioned in Cell cultures and drug treatments. To evaluate DNA transfection rate or shRNA-silencing efficiency, transfected astrocytes were harvested for Western blots.

### Statistics

SigmaPlot, SigmaStat (Systat Software, Inc.), and Prism (GraphPad Software) were used for data display and statistical analysis. Significance is reported as $P < 0.05$, and data were expressed as mean ± SEM. Student *t* test, one-way ANOVA followed by a post hoc multiple comparison analysis based on the Dunnett's method, or two-way ANOVA followed by a post hoc multiple comparison analysis based on the Holm-Sidak method were used to determine significant levels between treatments and controls. The Kolmogorov-Smirnov test was used to determine the significance level of two distributions.

### Online supplemental material

Fig. S1 shows the effects of LPS on PTZ-induced seizure susceptibility and astrocyte activation are attenuated in *TLR4*$^{-/-}$ mice during a critical developmental period. Fig. S2 shows that LPS increases mEPSC frequency and amplitude, but does not affect mIPSC frequency and amplitude in neurons co-cultured with astrocytes. Fig. S3 shows that A/LPS promotes synaptogenesis and dendritic branching in cultured hippocampal neurons. Fig. S4 shows the effects of LPS on MAPK and NF-κB expressions in cultured astrocytes and neurons co-cultured with astrocytes. Table S1 shows the effects of LPS on synaptogenesis and dendritic branching in WT astrocyte co-cultured hippocampal neurons (DIV15) derived from WT, *TLR4*$^{+/-}$, and *TLR4*$^{-/-}$ littermate mice.


## Acknowledgments

We thank Dr. Yuehai Ke for SHP2$^{E76V}$ plasmids and Dr. Joseph LoTurco for *piggyBac* plasmids. We thank the excellent technical assistant of the Imaging Facility at Zhejiang University School of Medicine.

This work was supported by the Major Research Program from the Chinese Ministry of Science and Technology (grant 2013CB530902), the National Natural Science Foundation of China (grants 91132712, 81300979, 81571125, 81571088, 81221003, and 81521062), and the Natural Science Foundation of Zhejiang Province (grants LR12C09001 and Q13C090002).

The authors declare no competing financial interests.

Submitted: 12 May 2016
Revised: 30 August 2016
Accepted: 19 October 2016


## References


Allen, N.J., M.L. Bennett, L.C. Foo, G.X. Wang, C. Chakraborty, S.J. Smith, and B.A. Barres. 2012. Astrocyte glypicans 4 and 6 promote formation of excitatory synapses via GluA1 AMPA receptors. *Nature.* 486:410–414. http://dx.doi.org/10.1038/nature11059

Bai, J., R.L. Ramos, J.B. Ackman, A.M. Thomas, R.V. Lee, and J.J. LoTurco. 2003. RNAi reveals doublecortin is required for radial migration in rat neocortex. *Nat. Neurosci.* 6:1277–1283. http://dx.doi.org/10.1038/nn1153

Bedner, P., A. Dupper, K. Hüttmann, J. Müller, M.K. Herde, P. Dublin, T. Deshpande, J. Schramm, U. Häussler, C.A. Haas, et al. 2015. Astrocyte uncoupling as a cause of human temporal lobe epilepsy. *Brain.* 138:1208–1222. http://dx.doi.org/10.1093/brain/awv067

Burda, J.E., and M.V. Sofroniew. 2014. Reactive gliosis and the multicellular response to CNS damage and disease. *Neuron.* 81:229–248. http://dx.doi.org/10.1016/j.neuron.2013.12.034

Chakravarty, S., and M. Herkenham. 2005. Toll-like receptor 4 on nonhematopoietic cells sustains CNS inflammation during endotoxemia, independent of systemic cytokines. *J. Neurosci.* 25:1788–1796. http://dx.doi.org/10.1523/JNEUROSCI.4268-04.2005

Chen, F., and J. LoTurco. 2012. A method for stable transgenesis of radial glia lineage in rat neocortex by *piggyBac* mediated transposition. *J. Neurosci. Methods.* 207:172–180. http://dx.doi.org/10.1016/j.jneumeth.2012.03.016

Chen, Y., A. Leask, D.J. Abraham, L. Kennedy, X. Shi-Wen, C.P. Denton, C.M. Black, L.S. Verjee, and M. Eastwood. 2011. Thrombospondin 1 is a key mediator of transforming growth factor β-mediated cell contractility in systemic sclerosis via a mitogen-activated protein kinase kinase (MEK)/extracellular signal-regulated kinase (ERK)-dependent mechanism. (published erratum appears in *Fibrogenesis Tissue Repair*. 2015. 8:4.] *Fibrogenesis Tissue Repair.* 4:9. http://dx.doi.org/10.1186/1755-1536-4-9

Christopherson, K.S., E.M. Ullian, C.C. Stokes, C.E. Mullowney, J.W. Hell, A. Agah, J. Lawler, D.F. Mosher, P. Bornstein, and B.A. Barres. 2005. Thrombospondins are astrocyte-secreted proteins that promote CNS synaptogenesis. *Cell.* 120:421–433. http://dx.doi.org/10.1016/j.cell.2004.12.020

Chung, W.S., L.E. Clarke, G.X. Wang, B.K. Stafford, A. Sher, C. Chakraborty, J. Joung, L.C. Foo, A. Thompson, C. Chen, et al. 2013. Astrocytes mediate synapse elimination through MEGF10 and MERTK pathways. *Nature.* 504:394–400. http://dx.doi.org/10.1038/nature12776

Chung, W.S., C.A. Welsh, B.A. Barres, and B. Stevens. 2015. Do glia drive synaptic and cognitive impairment in disease? *Nat. Neurosci.* 18:1539–1545. http://dx.doi.org/10.1038/nn.4142

Clarke, L.E., and B.A. Barres. 2013. Emerging roles of astrocytes in neural circuit development. *Nat. Rev. Neurosci.* 14:311–321. http://dx.doi.org/10.1038/nrn3484

Coulter, D.A., and C. Steinhäuser. 2015. Role of astrocytes in epilepsy. *Cold Spring Harb. Perspect. Med.* 5:a022434. http://dx.doi.org/10.1101/cshperspect.a022434

Devinsky, O., A. Vezzani, S. Najjar, N.C. De Lanerolle, and M.A. Rogawski. 2013. Glia and epilepsy: Excitability and inflammation. *Trends Neurosci.* 36:174–184. http://dx.doi.org/10.1016/j.tins.2012.11.008

Diamond, J.S. 2005. Deriving the glutamate clearance time course from transporter currents in CA1 hippocampal astrocytes: Transmitter uptake gets faster during development. *J. Neurosci.* 25:2906–2916. http://dx.doi.org/10.1523/JNEUROSCI.5125-04.2005

Djukic, B., K.B. Casper, B.D. Philpot, L.S. Chin, and K.D. McCarthy. 2007. Conditional knock-out of Kir4.1 leads to glial membrane depolarization, inhibition of potassium and glutamate uptake, and enhanced short-term synaptic potentiation. *J. Neurosci.* 27:11354–11365. http://dx.doi.org/10.1523/JNEUROSCI.0723-07.2007

Downer, E.J., D.G. Johnston, and M.A. Lynch. 2013. Differential role of Dok1 and Dok2 in TLR2-induced inflammatory signaling in glia. *Mol. Cell. Neurosci.* 56:148–158. http://dx.doi.org/10.1016/j.mcn.2013.04.007

Eroglu, C., and B.A. Barres. 2010. Regulation of synaptic connectivity by glia. *Nature.* 468:223–231. http://dx.doi.org/10.1038/nature09612

Eroglu, C., N.J. Allen, M.W. Susman, N.A. O'Rourke, C.Y. Park, E. Ozkan, C. Chakraborty, S.B. Mulinyawe, D.S. Annis, A.D. Huberman, et al. 2009. Gabapentin receptor alpha2delta-1 is a neuronal thrombospondin receptor responsible for excitatory CNS synaptogenesis. *Cell.* 139:380–392. http://dx.doi.org/10.1016/j.cell.2009.09.025

Fields, R.D., D.H. Woo, and P.J. Basser. 2015. Glial regulation of the neuronal connectome through local and long-distant communication. *Neuron.* 86:374–386. http://dx.doi.org/10.1016/j.neuron.2015.01.014

Foo, L.C., N.J. Allen, E.A. Bushong, P.B. Ventura, W.S. Chung, L. Zhou, J.D. Cahoy, R. Daneman, H. Zong, M.H. Ellisman, and B.A. Barres. 2011. Development of a method for the purification and culture of rodent astrocytes. *Neuron.* 71:799–811. http://dx.doi.org/10.1016/j.neuron.2011.07.022

Galic, M.A., K. Riazi, J.G. Heida, A. Mouihate, N.M. Fournier, S.J. Spencer, L.E. Kalynchuk, G.C. Teskey, and Q.J. Pittman. 2008. Postnatal inflammation increases seizure susceptibility in adult rats. *J. Neurosci.* 28:6904–6913. http://dx.doi.org/10.1523/JNEUROSCI.1901-08.2008

Gauthier, A.S., O. Furstoss, T. Araki, R. Chan, B.G. Neel, D.R. Kaplan, and F.D. Miller. 2007. Control of CNS cell-fate decisions by SHP-2 and its dysregulation in Noonan syndrome. *Neuron.* 54:245–262. http://dx.doi.org/10.1016/j.neuron.2007.03.027

Goldmann, T., P. Wieghofer, P.F. Müller, Y. Wolf, D. Varol, S. Yona, S.M. Brendecke, K. Kierdorf, O. Staszewski, M. Datta, et al. 2013. A new type of microglia gene targeting shows TAK1 to be pivotal in CNS autoimmune inflammation. *Nat. Neurosci.* 16:1618–1626. http://dx.doi.org/10.1038/nn.3531

Gorina, R., M. Font-Nieves, L. Márquez-Kisinousky, T. Santalucia, and A.M. Planas. 2011. Astrocyte TLR4 activation induces a proinflammatory environment through the interplay between MyD88-dependent NFκB signaling, MAPK, and Jak1/Stat1 pathways. *Glia.* 59:242–255. http://dx.doi.org/10.1002/glia.21094

Haydon, P.G., and M. Nedergaard. 2015. How do astrocytes participate in neural plasticity? *Cold Spring Harb. Perspect. Biol.* 7:a020438. http://dx.doi.org/10.1101/cshperspect.a020438

Hickey, E., H. Shi, G. Van Arsdell, and R. Askalan. 2011. Lipopolysaccharide-induced preconditioning against ischemic injury is associated with changes in toll-like receptor 4 expression in the rat developing brain. *Pediatr. Res.* 70:10–14. http://dx.doi.org/10.1203/PDR.0b013e31821d02aa

Hirschhorn, J., S. Mohanty, and N.R. Bhat. 2014. The role of tumor progression locus 2 protein kinase in glial inflammatory response. *J. Neurochem.* 128:919–926. http://dx.doi.org/10.1111/jnc.12522

Ikeda, H., M. Miyatake, N. Koshikawa, K. Ochiai, K. Yamada, A. Kiss, M.J. Donlin, W.M. Panneton, J.D. Churchill, M. Green, et al. 2010. Morphine modulation of thrombospondin levels in astrocytes and its implications for neurite outgrowth and synapse formation. *J. Biol. Chem.* 285:38415–38427. http://dx.doi.org/10.1074/jbc.M110.109827

Jack, C.S., N. Arbour, J. Manusow, V. Montgrain, M. Blain, E. McCrea, A. Shapiro, and J.P. Antel. 2005. TLR signaling tailors innate immune responses in human microglia and astrocytes. *J. Immunol.* 175:4320–4330. http://dx.doi.org/10.4049/jimmunol.175.7.4320

Jaworski, J., L.C. Kapitein, S.M. Gouveia, B.R. Dortland, P.S. Wulf, I. Grigoriev, P. Camera, S.A. Spangler, P. Di Stefano, J. Demmers, et al. 2009. Dynamic microtubules regulate dendritic spine morphology and synaptic plasticity. *Neuron.* 61:85–100. http://dx.doi.org/10.1016/j.neuron.2008.11.013

Lampron, A., A. Elali, and S. Rivest. 2013. Innate immunity in the CNS: Redefining the relationship between the CNS and Its environment. *Neuron.* 78:214–232. http://dx.doi.org/10.1016/j.neuron.2013.04.005

Lee, S.H., A. Simonetta, and M. Sheng. 2004. Subunit rules governing the sorting of internalized AMPA receptors in hippocampal neurons. *Neuron.* 43:221–236. http://dx.doi.org/10.1016/j.neuron.2004.06.015

Lee, Y.S., D. Ehninger, M. Zhou, J.Y. Oh, M. Kang, C. Kwak, H.H. Ryu, D. Butz, T. Araki, Y. Cai, et al. 2014. Mechanism and treatment for learning and memory deficits in mouse models of Noonan syndrome. *Nat. Neurosci.* 17:1736–1743. http://dx.doi.org/10.1038/nn.3863

Lehnardt, S., C. Lachance, S. Patrizi, S. Lefebvre, P.L. Follett, F.E. Jensen, P.A. Rosenberg, J.J. Volpe, and T. Vartanian. 2002. The toll-like receptor TLR4 is necessary for lipopolysaccharide-induced oligodendrocyte injury in the CNS. *J. Neurosci.* 22:2478–2486.

Li, S., L. Wang, Q. Zhao, Y. Liu, L. He, Q. Xu, X. Sun, L. Teng, H. Cheng, and Y. Ke. 2014. SHP2 positively regulates TGFβ1-induced epithelial-mesenchymal transition modulated by its novel interacting protein Hook1. *J. Biol. Chem.* 289:34152–34160. http://dx.doi.org/10.1074/jbc.M113.546077

Maroso, M., S. Balosso, T. Ravizza, J. Liu, E. Aronica, A.M. Iyer, C. Rossetti, M. Molteni, M. Casalgrandi, A.A. Manfredi, et al. 2010. Toll-like receptor 4 and high-mobility group box-1 are involved in ictogenesis and can be targeted to reduce seizures. *Nat. Med.* 16:413–419. http://dx.doi.org/10.1038/nm.2127

McCarthy, K.D., and J. de Vellis. 1980. Preparation of separate astroglial and oligodendroglial cell cultures from rat cerebral tissue. *J. Cell Biol.* 85:890–902. http://dx.doi.org/10.1083/jcb.85.3.890

Molofsky, A.V., R. Krencik, E.M. Ullian, H.H. Tsai, B. Deneen, W.D. Richardson, B.A. Barres, and D.H. Rowitch. 2012. Astrocytes and disease: a neurodevelopmental perspective. (published erratum appears in *Genes Dev.* 2012. 26:1508.) *Genes Dev.* 26:891–907. http://dx.doi.org/10.1101/gad.188326.112

Navarro-Quiroga, I., R. Chittajallu, V. Gallo, and T.F. Haydar. 2007. Long-term, selective gene expression in developing and adult hippocampal pyramidal neurons using focal in utero electroporation. *J. Neurosci.* 27:5007–5011. http://dx.doi.org/10.1523/JNEUROSCI.0867-07.2007

Okun, E., K.J. Griffioen, and M.P. Mattson. 2011. Toll-like receptor signaling in neural plasticity and disease. *Trends Neurosci.* 34:269–281. http://dx.doi.org/10.1016/j.tins.2011.02.005

Ortinski, P.I., J. Dong, A. Mungenast, C. Yue, H. Takano, D.J. Watson, P.G. Haydon, and D.A. Coulter. 2010. Selective induction of astrocytic gliosis generates deficits in neuronal inhibition. *Nat. Neurosci.* 13:584–591. http://dx.doi.org/10.1038/nn.2535

Pyka, M., C. Busse, C. Seidenbecher, E.D. Gundelfinger, and A. Faissner. 2011. Astrocytes are crucial for survival and maturation of embryonic hippocampal neurons in a neuron-glia cell-insert coculture assay. *Synapse.* 65:41–53. http://dx.doi.org/10.1002/syn.20816

Rakhade, S.N., and F.E. Jensen. 2009. Epileptogenesis in the immature brain: Emerging mechanisms. *Nat. Rev. Neurol.* 5:380–391. http://dx.doi.org/10.1038/nrneurol.2009.80

Ramanan, N., Y. Shen, S. Sarsfield, T. Lemberger, G. Schütz, D.J. Linden, and D.D. Ginty. 2005. SRF mediates activity-induced gene expression and synaptic plasticity but not neuronal viability. *Nat. Neurosci.* 8:759–767. http://dx.doi.org/10.1038/nn1462

Ramos, R.L., J. Bai, and J.J. LoTurco. 2006. Heterotopia formation in rat but not mouse neocortex after RNA interference knockdown of DCX. *Cereb. Cortex.* 16:1323–1331. http://dx.doi.org/10.1093/cercor/bhj074

Riazi, K., M.A. Galic, and Q.J. Pittman. 2010. Contributions of peripheral inflammation to seizure susceptibility: Cytokines and brain excitability. *Epilepsy Res.* 89:34–42. http://dx.doi.org/10.1016/j.eplepsyres.2009.09.004

Rivest, S. 2009. Regulation of innate immune responses in the brain. *Nat. Rev. Immunol.* 9:429–439. http://dx.doi.org/10.1038/nri2565

Robel, S., and H. Sontheimer. 2016. Glia as drivers of abnormal neuronal activity. *Nat. Neurosci.* 19:28–33. http://dx.doi.org/10.1038/nn.4184

Robel, S., S.C. Buckingham, J.L. Boni, S.L. Campbell, N.C. Danbolt, T. Riedemann, B. Sutor, and H. Sontheimer. 2015. Reactive astrogliosis causes the development of spontaneous seizures. *J. Neurosci.* 35:3330–3345. http://dx.doi.org/10.1523/JNEUROSCI.1574-14.2015

Rodgers, K.M., M.R. Hutchinson, A. Northcutt, S.F. Maier, L.R. Watkins, and D.S. Barth. 2009. The cortical innate immune response increases local neuronal excitability leading to seizures. *Brain.* 132:2478–2486. http://dx.doi.org/10.1093/brain/awp177

Seifert, G., K. Hüttmann, D.K. Binder, C. Hartmann, A. Wyczynski, C. Neusch, and C. Steinhäuser. 2009. Analysis of astroglial $K^+$ channel expression in the developing hippocampus reveals a predominant role of the Kir4.1 subunit. *J. Neurosci.* 29:7474–7488. http://dx.doi.org/10.1523/JNEUROSCI.3790-08.2009

Shen, Y., A.K. Lindemeyer, I. Spigelman, W. Sieghart, R.W. Olsen, and J. Liang. 2011. Plasticity of $GABA_A$ receptors after ethanol pre-exposure in cultured hippocampal neurons. *Mol. Pharmacol.* 79:432–442. http://dx.doi.org/10.1124/mol.110.068650

Shen, Y., A.K. Lindemeyer, C. Gonzalez, X.M. Shao, I. Spigelman, R.W. Olsen, and J. Liang. 2012. Dihydromyricetin as a novel anti-alcohol intoxication medication. *J. Neurosci.* 32:390–401. http://dx.doi.org/10.1523/JNEUROSCI.4639-11.2012

Sherwin, C., and R. Fern. 2005. Acute lipopolysaccharide-mediated injury in neonatal white matter glia: Role of TNF-alpha, IL-1beta, and calcium. *J. Immunol.* 175:155–161. http://dx.doi.org/10.4049/jimmunol.175.1.155

Sholl, D.A. 1953. Dendritic organization in the neurons of the visual and motor cortices of the cat. *J. Anat.* 87:387–406.

Simard, A.R., and S. Rivest. 2005. Do pathogen exposure and innate immunity cause brain diseases? *Neurol. Res.* 27:717–725. http://dx.doi.org/10.1179/016164105X49526

Sloan, S.A., and B.A. Barres. 2014. Mechanisms of astrocyte development and their contributions to neurodevelopmental disorders. *Curr. Opin. Neurobiol.* 27:75–81. http://dx.doi.org/10.1016/j.conb.2014.03.005

Téllez-Zenteno, J.F., S. Matijevic, and S. Wiebe. 2005. Somatic comorbidity of epilepsy in the general population in Canada. *Epilepsia.* 46:1955–1962. http://dx.doi.org/10.1111/j.1528-1167.2005.00344.x

Vezzani, A., B. Lang, and E. Aronica. 2015. Immunity and inflammation in epilepsy. *Cold Spring Harb. Perspect. Med.* 6:a022699. http://dx.doi.org/10.1101/cshperspect.a022699

Wetherington, J., G. Serrano, and R. Dingledine. 2008. Astrocytes in the epileptic brain. *Neuron.* 58:168–178. http://dx.doi.org/10.1016/j.neuron.2008.04.002

Xu, D., and C.K. Qu. 2008. Protein tyrosine phosphatases in the JAK/STAT pathway. *Front. Biosci.* 13:4925–4932. http://dx.doi.org/10.2741/3051

Xu, J., N. Xiao, and J. Xia. 2010. Thrombospondin 1 accelerates synaptogenesis in hippocampal neurons through neuroligin 1. *Nat. Neurosci.* 13:22–24. http://dx.doi.org/10.1038/nn.2459

Zhang, C., D. Atasoy, D. Araç, X. Yang, M.V. Fucillo, A.J. Robison, J. Ko, A.T. Brunger, and T.C. Südhof. 2010. Neurexins physically and functionally interact with GABA(A) receptors. *Neuron.* 66:403–416. http://dx.doi.org/10.1016/j.neuron.2010.04.008

Zhang, Y., S.A. Sloan, L.E. Clarke, C. Caneda, C.A. Plaza, P.D. Blumenthal, H. Vogel, G.K. Steinberg, M.S. Edwards, G. Li, et al. 2016. Purification and characterization of progenitor and mature human astrocytes reveals transcriptional and functional differences with mouse. *Neuron.* 89:37–53. http://dx.doi.org/10.1016/j.neuron.2015.11.013

Zhou, Y.D., S. Lee, Z. Jin, M. Wright, S.E. Smith, and M.P. Anderson. 2009. Arrested maturation of excitatory synapses in autosomal dominant lateral temporal lobe epilepsy. *Nat. Med.* 15:1208–1214. http://dx.doi.org/10.1038/nm.2019